Title: Oxygen and hydrogen isotopic evidence that Kama‘ehuakanaloa (Lō‘ihi) Seamount hydrothermal systems are recharged by deep Pacific seawater

Authors: Eric W. Chan[1*†], Brianna. A. Alanis[1], Christopher R. German[2], Darlene S. S. Lim[3], John. A. Breier[1]

[1] School of Earth, Environmental, and Marine Sciences, The University of Texas Rio Grande Valley, Edinburg, Texas, 78539, USA.
[2] Woods Hole Oceanographic Institution, Woods Hole, Massachusetts, 02543, USA.
[3] Space Science and Astrobiology Division, NASA Ames Research Center, Moffett Field, California, 94035, USA

*Corresponding author: Eric Chan (erik.w.chan@gmail.com)
†Present address: Picarro Inc., 3105 Patrick Henry Drive, Santa Clara, California 95054, USA.

Highlights:

- $\delta^{18}O$ and $\delta^{2}H$ isotopic ratios indicate Kama‘ehuakanaloa hydrothermal recharge entrains Pacific Bottom Water.
- Crater floor vent fluids exhibit isotopic values most similar to seawater from >4500 m.
- Data indicate multiple subsurface transport paths and thermal histories.
- Data suggest additional diffuse flow or water/mineral reactions in Pele's Pit.

Abstract

We observed negative and positive $\delta^{18}O$ and $\delta^{2}H$ deviations from fluids collected at Kama‘ehuakanaloa (previously known as Lō‘ihi) seamount relative to Pacific seawater from the same depth. Hydrothermal vents on the crater floor of Pele’s Pit at Kama‘ehuakanaloa, at a depth of 1320 m, had $\delta^{18}O$ and $\delta^{2}H$ values as low as -0.19‰ and -0.3‰, respectively. Seawater collected within the caldera, within a zone 45 m above the crater floor, had $\delta^{18}O$ and $\delta^{2}H$ values as high as 1.15‰ and 6.5‰, respectively. In comparison, Pacific seawater at 1200 m and 1400 m at nearby station ALOHA exhibit intermediate $\delta^{18}O$ and $\delta^{2}H$ values of 0.2‰ and 0.34‰. The high $\delta^{18}O$ and $\delta^{2}H$ values observed in the caldera water-column may be explained by isotopic modification processes, including water-rock reactions. However, we did not observe a vent source with similar isotopic composition; this suggests that substantial hydrothermal flow is entering the caldera through unidentified sources, potentially individually small but collectively important. Further, the low $\delta^{18}O$ and $\delta^{2}H$ values of the crater floor vents cannot be readily explained by isotopic modification processes alone. We conclude the crater floor vents predominantly reflect the isotopic composition of the Pacific seawater entrained into the hydrothermal system. Our observations suggest recharging seawater is entrained from below >4500 m, in the zone of Pacific Bottom Water. These findings illustrate the heterogeneity of hydrothermal transport processes at a volcanic seamount and how seamount hydrothermal convection can provide a mechanism that may contribute to vertical ocean mixing by transporting deep bottom waters to intermediate ocean depths.

Key Words: Stable isotopes in water, $\delta^{18}O$, $\delta^{2}H$, Kama‘ehuakanaloa, Lō‘ihi, hydrothermal

1. Introduction

Hydrothermal discharge to the ocean has long been recognized as an important biogeochemical process that influences numerous biogeochemical cycles, fuels chemosynthetic seafloor ecosystems, and may have played an important role in the development of our biosphere (Canfield et al., 2008; Edwards et al., 2005; Elderfield and Schultz, 1996). Hydrothermal discharge involves a complex set of coupled physical, chemical, and biological processes that are still not completely understood (Anantharaman et al., 2016; Breier et al., 2012; German and Seyfried, 2014). Notwithstanding, evidence is mounting that hydrothermal discharge represents an important component of the marine iron cycle and contributes to this micronutrient's oceanic distribution (Tagliabue et al., 2017).

Submarine hydrothermal discharge results from the thermally driven flow of seawater through the seafloor. Hydrothermal recharge arises wherever seawater is entrained into the sub-seafloor convection cell. Subsurface water-rock reactions and magmatic inputs can highly alter the initial seawater chemistry. Hydrothermal discharge is challenging to study, particularly over the full range of length and time scales over which important processes occur. However, hydrothermal discharge does produce observable effects in the water-column, and on that basis, investigations have been able to proceed. Hydrothermal recharge is much more challenging to observe and quantify because all gradients and related processes occur below the seafloor and are likely dispersed over much greater length scales than those associated with hydrothermal discharge (Johnson et al., 2010). Accordingly, much less is known about hydrothermal recharge than about hydrothermal discharge.

What has been determined about hydrothermal recharge, to date, results from a combination of seismic studies, ocean drilling, heat flow measurements, and theoretical modeling (*e.g.*, Lowell and Yao, 2002; Fisher et al., 2003; Tsuji et al., 2012). While some aspects of fluid history can be deduced from the geochemistry of vent fluids at the point that they exit the seafloor, in most cases, information related to where recharge occurs is very difficult to constrain. The non-conservative chemical constituents of recharging seawater are, consequently, also difficult to constrain.

Even the O and H isotopic compositions of recharging seawater can be modified by geochemical reactions and modifications that can occur if hydrothermal systems reach sufficiently high temperatures (Böhlke and Shanks, 1994; Bowers and Taylor, 1985; Jean-Baptiste et al., 1997). Measurements from numerous mid-ocean ridge systems globally have shown that high-temperature vent fluids are typically enriched in ^{18}O relative to ambient seawater and that these fluids are a source of ^{18}O to the oceans (Jean-Baptiste et al., 1997). While less widely reported, measurements of ^{2}H also show enrichments relative to seawater in most cases of high-temperature venting that have been investigated (Shanks et al., 1995).

Nevertheless, the O and H isotopic compositions of seawater are inherent properties indicative of source and process history; and $\delta^{18}O$ and $\delta^{2}H$ values can provide deep insight into fluid transport and mixing processes in some situations. While the O and H isotopic composition of

hydrothermal fluids at mid-ocean ridges have been well studied, the isotopic composition of hydrothermal fluids at hotspot volcanoes is less well-known. In this study, we measured $\delta^{18}O$ and $\delta^{2}H$ values of fluids from Kama‘ehuakanaloa (previously known as Lō‘ihi) seamount and the background Pacific Ocean to better understand the origin of hydrothermal recharge at this active hotspot volcano. Kama‘ehuakanaloa presents an opportunity to better understand the processes that entrain and modify seawater within hydrothermal systems and represents a unique contrast to better studied mid-ocean ridge systems.

Kama‘ehuakanaloa Seamount (18° 54' 24.1056" N, 155° 15' 27.09" W), is a young seismically active intraplate underwater hotspot volcano that rises ~4 km above the Pacific abyssal plain (Glazer and Rouxel, 2009; Karl et al., 1989). The last known eruption at Kama‘ehuakanaloa was in 1996 (Garcia et al., 1998); however, an eruption was ongoing at Kīlauea during this study (Neal et al., 2019). Focused and diffuse hydrothermal venting is known to occur in the most southwest of three calderas, referred to as Pele’s Pit (Fig. 1) (Duennenbier et al. 1997). Kama‘ehuakanaloa is of particular interest because its low sulfide, high iron vent chemistry discharges into low dissolved oxygen ambient seawater, which inhibits iron precipitation and promotes retention of dissolved iron in the plume (Sedwick et al. 1992; Paulmier and Ruiz-Pino, 2009; Toner et al., 2012; Rouxel et al., 2018). As a result, Kama‘ehuakanaloa dissolved iron can travel far: Jenkins et al., (2020) observed the Kama‘ehuakanaloa iron signal as far as 1000 km from the seamount and their modeling suggests Kama‘ehuakanaloa iron may be transported so far as to influence the primary productivity in the shallow waters of the northwest Pacific. Thus, hydrothermal processes at this submarine volcano may influence ocean chemistry over a wide region of the Pacific, and in this study, we seek to better understand how seawater flows through this hydrothermal system as a precursor to better quantifying the export fluxes of water and solutes from this seamount to the ocean.

2 Methods

2.1 Sample Collection

During 23 August to 11 September 2018, we collected samples from low temperature hydrothermal vents and the water-column at Kama‘ehuakanaloa Seamount (18° 54-55' N, 155° 15-16' W) during E/V *Nautilus* cruise NA100. The samples were from (i) vent sites within and around Pele’s Pit (*e.g.,* Fig. 2a-c), (ii) the water-column within the caldera overlying the vents (*e.g.,* Fig. 2d), and (iii) a background seawater sample to the north of the Summit removed from any known hydrothermal sources (Figure 1). The vent sites sampled were at Markers 31, 34, and 38 (Fig. 2a, referred to collectively in this paper as Crater Floor Vents), and Markers 2 and 57 (Fig. 2b, referred to as Crater Rim Vents) from Davis and Clague, (1998) and Glazer and Rouxel, (2009), and an area of discharge from a cluster of smaller vent structures that we refer to as “Chimlets” (Fig. 2c) that are near the *Spillway* referred to in Glazer and Rouxel, (2009). The samples collected within the caldera water-column (*e.g.,* Fig 2d) were all within 210 m of the caldera floor, which sits at a depth of 1320 m. Samples were collected using an *in-situ* water and particulate sampling system mounted on ROV *Hercules*. This sample collection system consists of a multiport valve, water and filter holders, a flowmeter, and a pump connected to an intake wand held in the ROV manipulator (Breier et al., 2014); this tool enables targeted

sampling at seafloor vents and seeps as well as in the overlying water-column. The sampler was used to collect duplicate water samples for $\delta^{18}O$ and $\delta^{2}H$ analyses. The sampling system was prefilled with distilled/deionized (DI) water prior to deployment to prevent implosion. This DI water was purged during sample collection by flushing with seven times the sample volume (Breier et al., 2014); to verify this occurred, operational DI water blanks were collected for analysis. Fluid temperature measurement readings for Crater Floor, Crater Rim, and Chimlet samples were taken with a high-temperature thermocouple probe mounted on the sampler intake wand (Fornari et al., 1997). Temperature measurement readings for “Caldera seawater” samples, and temperature and salinity measurements for background seawater samples, were taken with a Seabird Scientific 49 FastCat CTD.

During January 2020, we collected a full ocean depth set of Pacific water-column samples from a site 513 km to the northwest, at station ALOHA (A Long-Term Oligotrophic Habitat Assessment; 22° 45'N, 158° 00' W) during Hawaii Ocean Time-Series (HOT) cruise 318. Duplicate samples were collected between 5 and 4800 m during multiple hydrocasts using a 24-bottle CTD water sampling rosette.

138

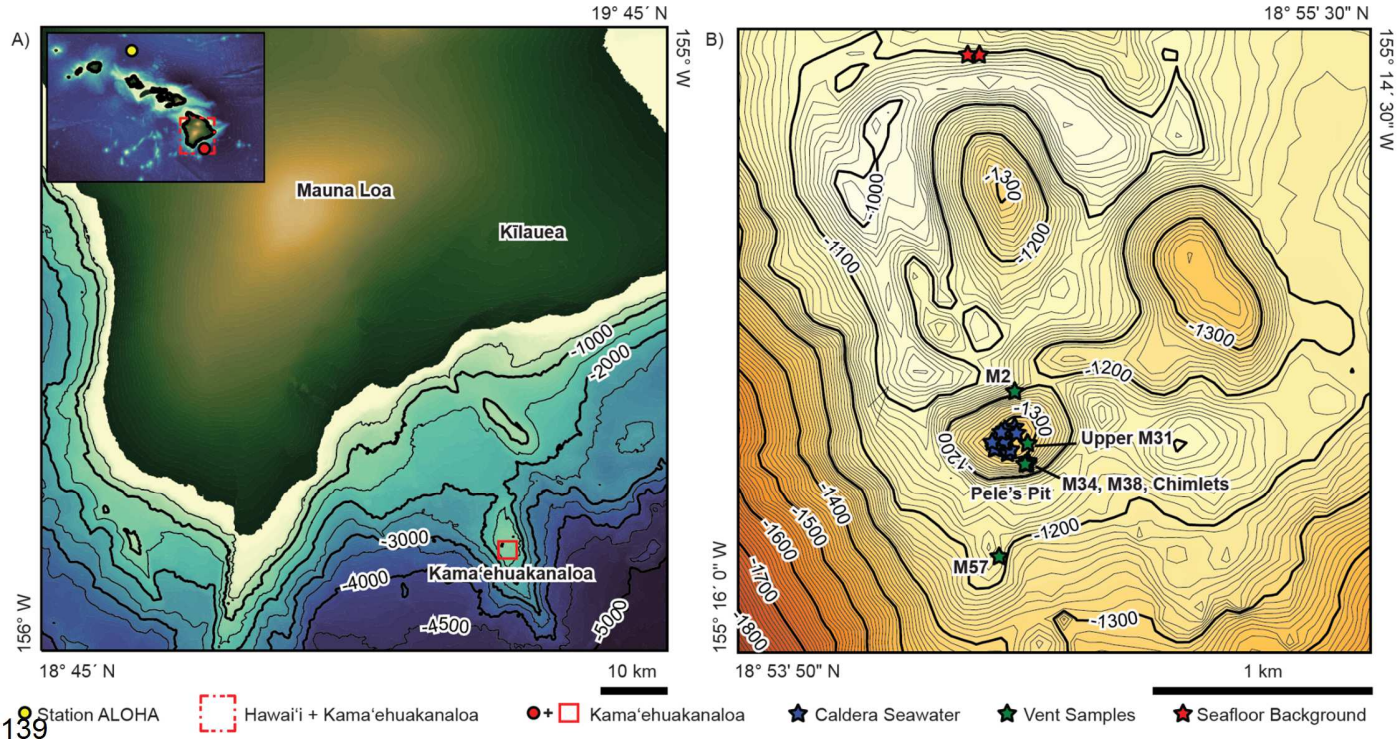

139

140 **Fig. 1. Maps of Kama‘ehuakanaloa Seamount.** A.) Regional map showing the Island of
141 Hawai‘i and the Kama‘ehuakanaloa Seamount summit (enclosed in a solid red rectangle) with
142 bathymetry contours at 500 m intervals, and an inset map showing the location of
143 Kama‘ehuakanaloa Seamount (red circle) and Station ALOHA (yellow circle). B.)
144 Kama‘ehuakanaloa summit map showing Pele’s Pit caldera and the location of caldera
145 seawater samples (blue stars), vent fluid samples (green stars), and seafloor background
146 seawater samples (red stars). Bathymetry contours at 10 m intervals and marked at 100 m
147 intervals. Bathymetry is from (Ryan et al., 2009).

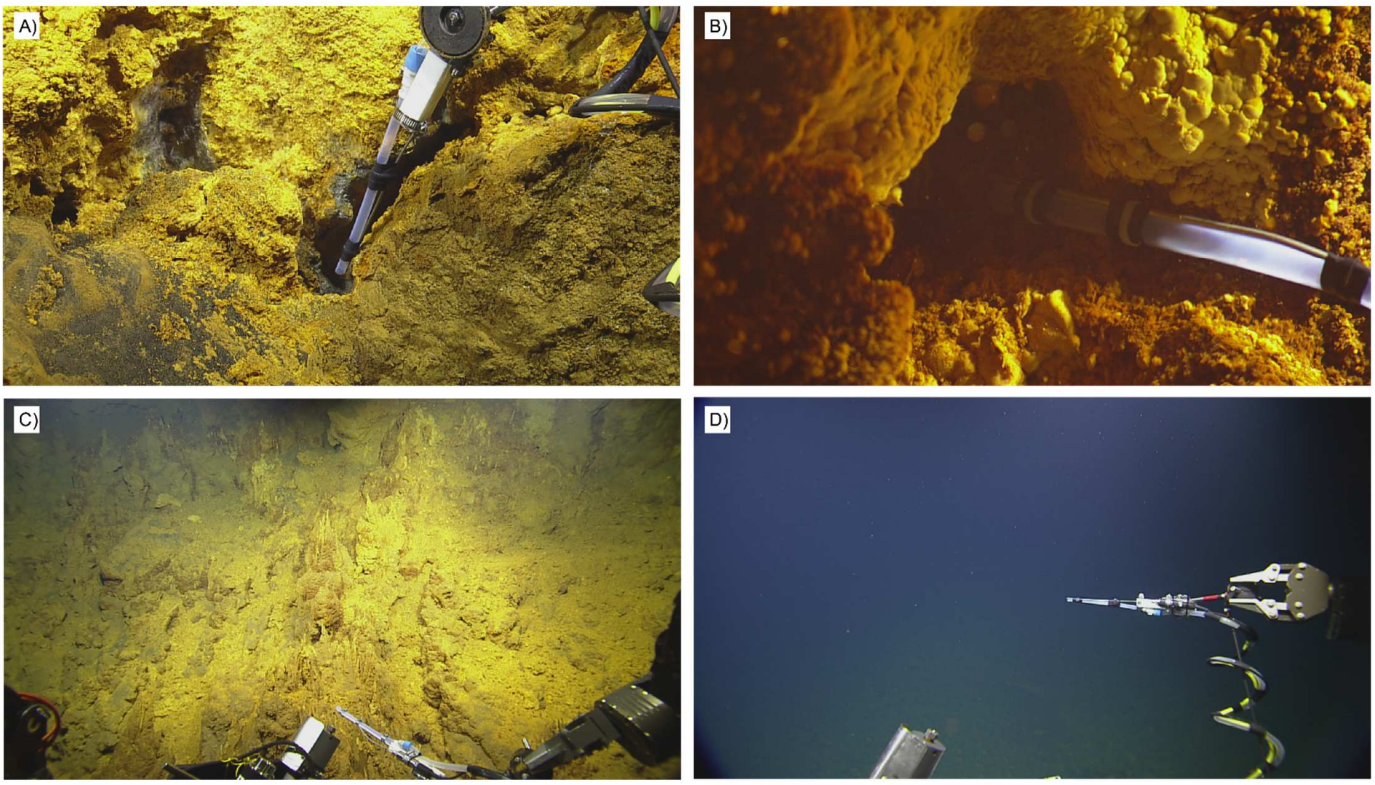

[Color image intended for double column width 190 mm, shown at 100% scale]

Fig. 2. Images of Vent Sites and Sampling. A.) Crater Floor and B.) Crater Rim vent sampling with SUPR sampler intake and temperature probe positioned within vent orifice by ROV manipulator. C.) The cluster of vent structures in the Chimlet vent area were too small and fragile to sample directly so the sampler intake and temperature probe were positioned immediately above the point of fluid outflow from these structures. D.) Samples were also taken from multiple locations within the caldera water column and outside the caldera near the surface of the seamount using these same tools.

[Color image intended for double column width 190 mm, shown at 100% scale]

2.2 Sample Analysis

We analyzed samples for $\delta^{18}O$ and $\delta^{2}H$ of water on a Picarro G2410-i cavity ring-down spectrometer with a water vaporizer module and autosampler (Walker et al., 2016). Our measurements are reported as δ values, in per mil (‰) units, where $\delta = 10^3[(R/R_{VSMOW2})-1]$ and R is the isotopic ratio of $^{18}O/^{16}O$ or $^{2}H/^{1}H$, respectively. We calibrated these measurements using VSMOW2 and SLAP2 isotopic standards: VSMOW2 ($\delta^{18}O$ = 0‰ ± 0.02‰, $\delta^{2}H$ = 0‰ ± 0.3‰) and SLAP2 ($\delta^{18}O$ = -55.50 ‰ ± 0.02‰, $\delta^{2}H$ = -427.5‰ ± 0.03‰) (Lin et al., 2010). We used Picarro's Chemcorrect software to identify and quantify spectral interferences from contaminants including trace hydrocarbons (Walker et al., 2016). To avoid memory effects within the spectrometer, we measured each sample at least seven times and determined the

$\delta^{18}O$ and $\delta^{2}H$ values as the average of the last three measurements. We use the term “lighter” to describe lower δ values representing samples depleted in ^{18}O or ^{2}H, and “heavier" to describe higher δ values representing samples enriched in ^{18}O or ^{2}H.

2.3 Analysis & Calculations

K-means clustering analysis of sample data from Station ALOHA was carried out with Python and several supporting packages. K-means is a Bayesian algorithm that forms clusters based on data similarity from the Scikit-Learn Python package (Pedregosa et al., 2011). *K* is the hyperparameter that determines how many clusters are generated by the algorithm and is the only user-input parameter for this method. The cluster assignments are graded by the sum of squared error (SSE) of the Euclidean distances between the data instance and the centroid. Since the SSE is a measure of variance, the purpose of K-means is to minimize this value to obtain the best clustering.

The isotopic composition of mixtures of seawater and vent fluid is estimated assuming simple conservative mixing between seawater and vent fluid using the following equation with $\delta^{18}O$ values as examples:

Equation 1:

$$VFF = \frac{(\delta^{18}O_{mix} - \delta^{18}O_{sw})}{(\delta^{18}O_{vf} - \delta^{18}O_{sw})}$$

where VFF represents the vent fluid fraction in a sample mixture, $\delta^{18}O_{mix}$ is the δ value of the sample mixture, $\delta^{18}O_{sw}$ is the δ value of seawater, and $\delta^{18}O_{vf}$ is the δ value of the vent fluid.

3. Results

All measurement values for station ALOHA samples are reported in Table 1 and all values for Kama‘ehuakanaloa samples are reported in Table 2. All Kama‘ehuakanaloa samples were isotopically heavier than the average of the operational blanks, which were -0.76‰ for $\delta^{18}O$ and -4.1‰ for $\delta^{2}H$. The operational blanks consisted of the distilled/deionized water from the ship used to pre-fill the sampling system. The fact that all samples were heavier than the operational blanks confirms that sample collection worked as intended.

Measured $\delta^{18}O$ and $\delta^{2}H$ values for all samples collected at Station ALOHA are shown in Figure 3. These measurements illustrate the isotopic structure of the Pacific Ocean in this region, including the trend to lighter isotopic $\delta^{18}O$ and $\delta^{2}H$ values with depth. Specifically, both $\delta^{18}O$ and $\delta^{2}H$ decrease sharply from the surface to 500 m, decrease relatively little from 500 m to 4500 m and decrease sharply again from 4500 to the bottom. $\delta^{18}O$ values range from +0.87‰ in the surface ocean to -0.29‰ at 4800 m, the deepest depth measured. $\delta^{2}H$ values range from +7.9‰ in the surface layer to -1.9‰ at 4800 m. The one exception to this trend is the sample collected from 2600 m, which has a $\delta^{18}O$ value of +3.7‰ and is notably heavier than the prevailing trend. For both isotopic ratios, the shallowest samples are isotopically the heaviest but exhibit steep gradients to lighter values with increasing depth to 500 m. Between water

depths of 500 m to 4000 m there is comparatively little variation in either isotopic ratio, with $\delta^{18}O$ values trending slightly lighter with increasing depth, while $\delta^{2}H$ values remain relatively constant. For both isotopic ratios, the deepest samples from below 4000 m are isotopically the lightest with notably steep gradients below 4500 m to the lightest values at the deepest depths. In both isotope systems, negative ratios are only observed below 4000m.

Measured $\delta^{18}O$ and $\delta^{2}H$ values for all samples collected at Kama'ehuakanaloa are shown in Figure 4, along with summary boxplots of the values for the Pacific water-column profile (panels C & D). We can identify four different groups within the Kama'ehuakanaloa samples based on their proximity to venting, location, depth in the water-column, and $\delta^{18}O$ and $\delta^{2}H$ values. The seawater samples collected within the caldera of Pele's pit, but not in close proximity to a vent, are referred to as "Caldera seawater" samples. Samples collected from vents at or beyond the rim of the caldera, at marker 2 to the north and marker 57 to the south, are referred to as "Crater Rim" samples. Samples collected from vents on the floor of the caldera, at markers 31, 34, and 38, are referred to as "Crater Floor" samples. Samples collected approximately 1 m above the "Chimlets," which had active discharge but were individually too small to sample from directly, are referred to as "Chimlet" samples.

"Caldera seawater" samples have $\delta^{18}O$ values between +0.06‰ and +1.15‰ with an average of +0.38‰, and $\delta^{2}H$ values between +1.8‰ and +6.5‰ with an average of +4.0‰ (Fig. 4). The "Caldera seawater" samples include the heaviest $\delta^{18}O$ and $\delta^{2}H$ values observed at Kama'ehuakanaloa seamount in this study, these samples are from the bottom depths of the caldera below the crater rim (Fig. 4C & D). The temperatures of the "Caldera seawater" samples are indistinguishable from background seawater at this same depth at Station ALOHA in the North Pacific open ocean (Tables 1 and 2). By contrast, the two "Crater Rim" vent-samples have $\delta^{18}O$ and $\delta^{2}H$ values that are skewed to the lighter end of the "Caldera seawater" samples isotopic range and intermediate between ALOHA samples from the same depth and hydrothermal samples from the Pele's Pit crater floor (Fig. 4D). The temperatures of the "Crater Rim" vent-samples were 11.0°C and 11.5°C, respectively, which is ~ 7.5°C above background seawater (Table 2). The three "Chimlet" area samples have $\delta^{18}O$ values similar to the "Crater Rim" vent-fluids and $\delta^{2}H$ values somewhat heavier than the "Crater Rim" samples but still intermediate between station ALOHA at the same depth and the "Crater Floor" vents. The temperatures of the "Chimlet" samples range from that of background seawater to 15°C. The four "Crater Floor" samples have $\delta^{18}O$ values between -0.19‰ and +0.13‰ with an average of -0.05‰, and $\delta^{2}H$ values from -0.3‰ to +1.8‰ with an average of +0.9‰. The "Crater Floor" samples include the lightest $\delta^{18}O$ and $\delta^{2}H$ values observed at Kama'ehuakanaloa seamount in this study (Fig. 4C & D). The temperatures of the "Crater Floor" fluid samples were between 23.0°C and 40.4°C. A seafloor background sample collected away from any known areas of venting and outside of Pele's Pit caldera, 1.9 km to the north and at a depth of 1086 m, had a $\delta^{18}O$ value of +0.29‰, and $\delta^{2}H$ value of +3.7‰. These seafloor background samples at Kama'ehuakanaloa are isotopically indistinguishable (within error) from Station Aloha samples at the same depth.

Kama'ehuakanaloa "Caldera seawater" samples include those with $\delta^{18}O$ and $\delta^{2}H$ values that are isotopically heavier and lighter than Pacific Ocean seawater at the same depth as Pele's Pit

246 in direct contrast to the background samples collected to the north of the crater; the mean $\delta^{18}O$
247 and $\delta^{2}H$ values within the caldera are isotopically heavier than Pacific Ocean seawater at the
248 same depth. This can be seen in Fig. 4C by comparing “Caldera seawater” samples to Pacific
249 500 - 1500m depth seawater. For Kama‘ehuakanaloa “Crater Rim” and “Chimlet” samples, the
250 $\delta^{18}O$ values are isotopically similar to Pacific Ocean seawater at the same depth as Pele’s Pit.
251 However, the mean $\delta^{2}H$ values of Kama‘ehuakanaloa "Crater Rim" and “Chimlet” samples (Fig.
252 4D) are isotopically lighter than Pacific Ocean seawater at the same depth as Pele’s Pit. For
253 Kama‘ehuakanaloa "Crater Floor" samples, neither the $\delta^{18}O$ nor the $\delta^{2}H$ values correspond to
254 the isotopic composition of Pacific seawater at the depth of Pele’s Pit. Rather, the $\delta^{18}O$ and the
255 $\delta^{2}H$ values of Kama‘ehuakanaloa "Crater Floor" samples are most similar to the deepest Pacific
256 seawater from >4500 m (Figs. 3C & D, 4A, B, & C). "Crater Rim" $\delta^{2}H$ values are also most
257 similar to these deep Pacific seawater samples.

258

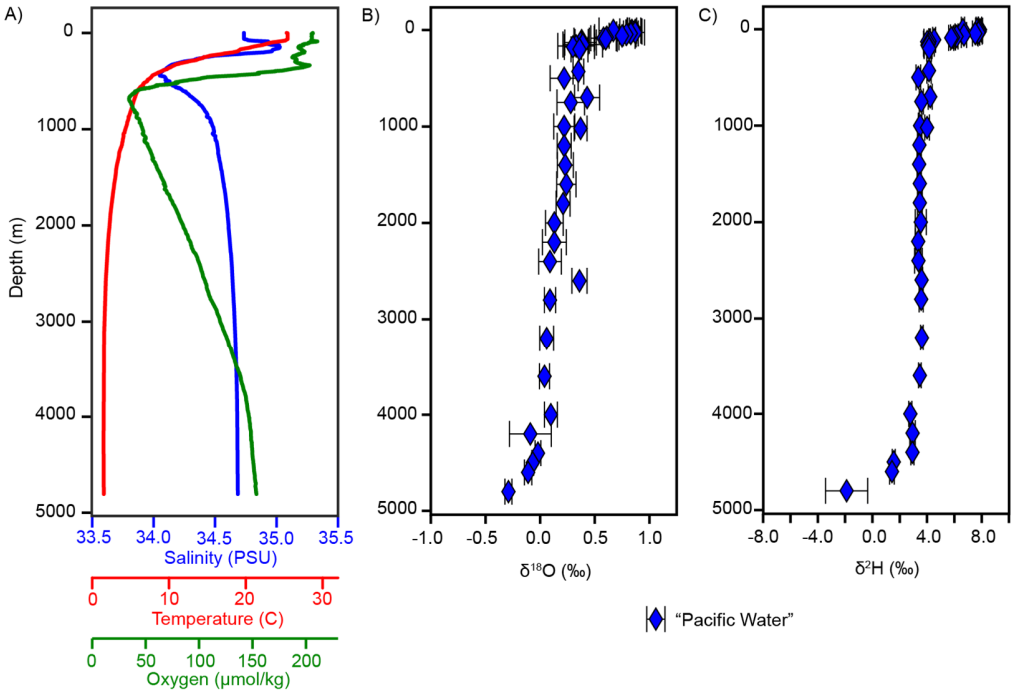

Fig. 3. Background Pacific Hydrography and Isotopic Composition. A.) Salinity (blue), temperature (red), and oxygen (green) profiles at Station ALOHA where "Pacific" samples were collected. B.) $\delta^{18}O$ profile of seawater samples taken at ALOHA station (blue diamonds). C.) $\delta^{2}H$ profile at station ALOHA (blue diamonds).

[Color image intended for 1.5 column width 140 mm, shown at 100% scale]

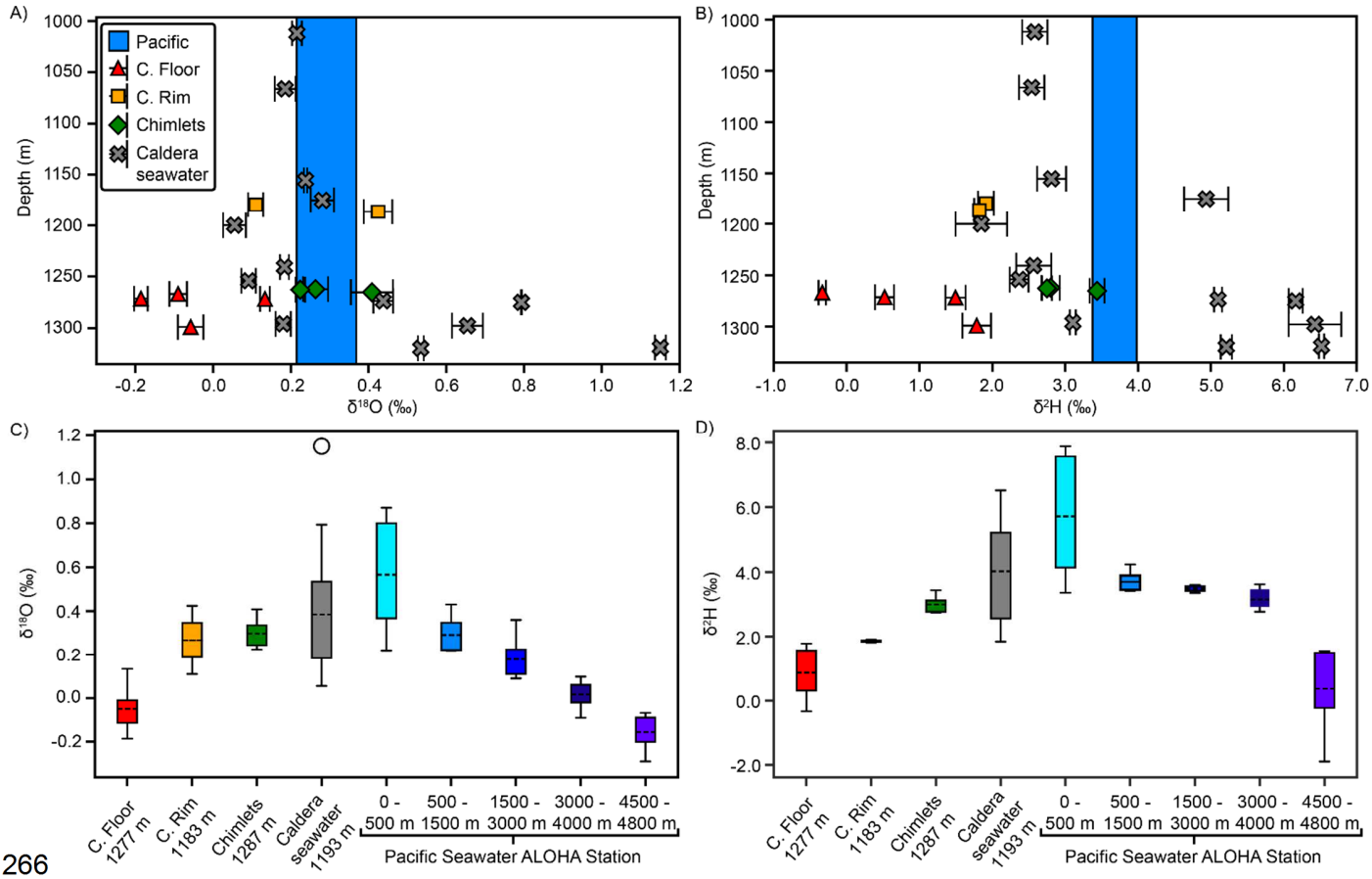

Fig. 4. Isotopic Composition of Kama‘ehuakanaloa Fluids and Pacific Seawater. A) $\delta^{18}O$ and B) $\delta^{2}H$ isotopic ratios of fluid samples respectively by depth. Red triangles: “Crater Floor” hydrothermal vent fluid $\delta^{18}O$ and $\delta^{2}H$ values characterized by temperatures from 23 to 40°C. Orange squares: “Crater Rim” $\delta^{18}O$ and $\delta^{2}H$ values characterized by lower temperatures of ~11°C. Green diamonds: “Chimlet” $\delta^{18}O$ and $\delta^{2}H$ values from samples collected above focused flow from chimlets located between marker 34 and 38. Gray X’s: “Caldera seawater” $\delta^{18}O$ and $\delta^{2}H$ values of samples collected inside the caldera but removed from direct vent influence. In subpanels A and B, blue shaded areas represent the range of $\delta^{18}O$ and $\delta^{2}H$ values of Pacific seawater samples from station ALOHA with respect to the same depth range of Kama‘ehuakanaloa hydrothermal samples; and error bars represent 1σ standard deviation estimates from duplicate measurements. C) $\delta^{18}O$ and D) $\delta^{2}H$ distributions of Kama‘ehuakanaloa hydrothermal samples and Pacific background water at ALOHA station. Pacific seawater samples from ALOHA station (cyan to purple bars) are grouped by water mass depths. Black dashed lines are the average for each boxplot. Each box extends vertically to the 1σ limits of the group sample population, and the whiskers extend to the 2σ limits. Data beyond the 2σ limits are shown as individual circles.

[Color image intended for double column width 190 mm, shown at 100% scale]

Depth (m)	$\delta^{18}O$ ‰	$\delta^{18}O$ σ	$\delta^{2}H$ ‰	$\delta^{2}H$ σ	Temperature (°C)	Salinity (PSU)	Dissolved O_2 (µM)
5	0.67	0.13	6.6	0.12	25.437	34.74	206.3
5	0.87	0.05	7.9	0.12	25.437	34.74	206.3
5	0.84	0.04	7.7	0.08	25.437	34.74	206.3
15	0.83	0.10	7.8	0.26	25.442	34.74	205.4
25	0.87	0.09	7.9	0.18	25.448	34.74	205.4
35	0.83	0.07	7.8	0.09	25.450	34.74	205.4
45	0.79	0.09	7.5	0.20	25.451	34.74	205.6
60	0.75	0.12	6.7	0.20	25.454	34.74	205.2
75	0.61	0.11	6.2	0.11	25.243	34.77	204.9
85	0.58	0.12	5.9	0.18	24.652	34.90	208.4
90	0.60	0.11	5.8	0.19	24.223	34.93	209.8
110	0.38	0.07	4.5	0.11	22.818	34.91	201.8
125	0.38	0.06	4.2	0.05	22.249	34.98	197.1
130	0.37	0.14	4.0	0.23	21.837	35.02	197.2
150	0.39	0.18	4.1	0.39	20.581	35.03	193.0
165	0.33	0.17	4.0	0.26	19.652	34.99	194.5
175	0.30	0.08	4.1	0.29	19.186	34.97	195.9
200	0.36	0.08	4.2	0.17	18.452	34.91	197.7
430	0.35	0.05	4.1	0.15	8.119	34.05	148.8
500	0.22	0.13	3.4	0.17	7.188	34.13	84.3
700	0.43	0.11	4.2	0.15	5.439	34.34	34.7
750	0.28	0.13	3.6	0.15	5.282	34.38	37.1
1000	0.22	0.10	3.5	0.12	4.316	34.49	47.1
1020	0.37	0.06	4.0	0.17	4.253	34.49	47.9
1200	0.22	0.06	3.4	0.14	3.711	34.52	53.5
1400	0.23	0.07	3.4	0.15	3.167	34.55	60.6
1600	0.24	0.09	3.5	0.11	2.834	34.57	68.5
1800	0.21	0.06	3.5	0.18	2.486	34.60	77.2
2000	0.13	0.08	3.5	0.41	2.270	34.61	85.0
2200	0.13	0.11	3.4	0.20	2.040	34.62	92.3
2400	0.09	0.10	3.4	0.28	1.870	34.64	100.4
2600	0.36	0.07	3.6	0.08	1.756	34.64	106.3
2800	0.09	0.05	3.6	0.15	1.676	34.65	112.4
3200	0.06	0.06	3.6	0.09	1.542	34.67	127.1
3600	0.04	0.05	3.5	0.09	1.482	34.68	139.1
4000	0.10	0.06	2.8	0.11	1.467	34.68	146.6
4200	-0.09	0.19	2.9	0.20	1.479	34.68	148.7
4400	-0.02	0.03	2.9	0.11	1.494	34.68	149.9
4500	-0.07	0.01	1.6	0.11	1.498	34.68	150.9
4600	-0.11	0.03	1.4	0.17	1.503	34.68	152.0
4800	-0.29	0.03	-1.9	1.55	1.513	34.69	153.7

Table 1. Background Pacific Isotopic Measurements and Hydrographic Data. $\delta^{18}O$ and $\delta^{2}H$ values from station ALOHA along with standard hydrographic data collected via CTD. Data collected from HOT cruise 318.

285

Type	Sample ID	Depth (m)	Latitude	Longitude	$\delta^{18}O$ ‰	$\delta^{18}O$ σ	$\delta^{2}H$ ‰	$\delta^{2}H$ σ	Fluid T. [1,2] (°C)	Background Seawater[2,3]			Sample Notes
										T. (°C)	Salinity (PSU)	Diss. O_2 (µM)	
Crater Floor Vents	NA100-089	1267	18.90555	-155.25698	-0.09	0.02	-0.3	0.05	38.7	4.203	34.48	51.4	M38
	NA100-022	1271	18.90559	-155.25694	-0.19	0.02	0.5	0.13	39.0	3.861	34.53	50.8	M34
	NA100-088	1272	18.90562	-155.25688	0.13	0.01	1.5	0.10	40.4	4.008	34.49	51.7	M34
	NA100-021	1299	18.90644	-155.25691	-0.06	0.03	1.8	0.20	23.0	3.850	34.52	50.5	M31 Upper
Crater Rim Vents	NA100-055	1179	18.90876	-155.25746	0.11	0.02	1.9	0.11	11.0	3.729	34.52	52.6	M2 Lower
	NA100-062	1186	18.90132	-155.25811	0.42	0.04	1.8	0.07	11.5	3.708	34.51	53.8	M57
Chimlet Area	NA100-091	1262	18.90555	-155.25698	0.26	0.03	2.8	0.10	3.8	3.769	34.50	51.8	
	NA100-092	1263	18.90555	-155.25697	0.22	0.01	2.7	0.07	3.8	3.784	34.50	51.7	
	NA100-090	1265	18.90555	-155.25698	0.41	0.05	3.4	0.10	15.0	3.819	34.50	51.5	
Caldera seawater	NA100-012	1012	18.90601	-155.25778	0.22	0.01	2.6	0.17	4.211	4.211	34.51	51.1	Above caldera
	NA100-047	1066	18.90619	-155.25765	0.19	0.03	2.5	0.17	4.059	4.059	34.50	47.4	Inside caldera
	NA100-048	1155	18.90697	-155.25807	0.24	0.01	2.8	0.20	3.849	3.849	34.51	49.7	Inside caldera
	NA100-013	1175	18.90655	-155.25846	0.28	0.03	4.9	0.30	3.836	3.836	34.54	51.5	Inside caldera
	NA100-014	1200	18.90621	-155.25825	0.06	0.03	1.8	0.35	3.834	3.834	34.53	45.7	Inside caldera
	NA100-049	1241	18.90698	-155.25806	0.18	0.01	2.6	0.20	3.805	3.805	34.52	50.7	Inside caldera
	NA100-015	1254	18.90621	-155.25834	0.09	0.02	2.4	0.13	3.830	3.830	34.53	50.4	Inside caldera
	NA100-050	1274	18.90695	-155.25804	0.44	0.03	5.1	0.05	3.814	3.814	34.52	50.8	Inside caldera
	NA100-016	1275	18.90650	-155.25786	0.79	0.00	6.2	0.10	3.881	3.881	34.53	50.5	Inside caldera
	NA100-051	1296	18.90711	-155.25788	0.18	0.02	3.1	0.04	3.828	3.828	34.52	51.8	Inside caldera
	NA100-017	1298	18.90654	-155.25784	0.65	0.04	6.4	0.40	3.843	3.843	34.53	50.5	Inside caldera
	NA100-018	1319	18.90691	-155.25737	1.15	0.01	6.5	0.03	3.841	3.841	34.53	50.5	Inside caldera
	NA100-052	1320	18.90722	-155.25745	0.53	0.01	5.2	0.08	3.851	3.851	34.52	51.7	Inside caldera
Background	NA100-058	1086	18.92385	-155.25903	0.29	0.038	3.7	0.08	4.041	4.041	34.50	48.5	Outside caldera

[1]Fluid temperature measurements reading for Crater Floor, Crater Rim, and Chimlet samples were taken with a high temperature thermocouple probe (Fornari et al., 1997).
[2]Temperature measurements readings for "Caldera seawater" samples and temperature and salinity measurements for background seawater samples were taken with a Seabird Scientific 49 FastCat CTD.
[3]Dissolved oxygen measurements were made with an Aanderaa 3830 optode.

Table 2. Isotopic Measurements of Kama'ehuakanaloa Fluids and Hydrographic Data. $\delta^{18}O$ and $\delta^{2}H$ values of Kama'ehuakanaloa fluid samples with corresponding fluid temperature measurements and local background hydrography data collected with ROV mounted sensors. For "Crater Floor", "Crater Rim", and "Chimlet" samples the fluid temperatures were measured at the inlet of the sampling system and represent temperatures of hydrothermal fluid exiting the vent. "Caldera seawater" water-column fluid temperatures were measured with a Sea-Bird FastCAT 39 mounted to the ROV. Sample notes identify focused vent names and for the "Caldera seawater" samples whether the samples were collected inside the caldera or above the caldera rim. In the case of focused vent sampling, the background seawater hydrography measurements represent the seawater the vent fluid is discharged into. In the case of the water-column measurements, the background hydrography measurements and fluid measurements are synonymous.

286

Type	Vent Sample	T. (°C)	Mg (mmol/kg)	Cl (mmol/kg)
Crater Floor Vents	M38	38	52.1	544
	M34	41	51.5	545
	M34	41	51.5	545
	M31 Upper	31	52.2	544
Crater Rim Vents	M2 Lower	22	52.7	542
	M57	17	54.5	539
Pele's Pit Seawater			52.7[1]	539

[1]Pele's Pit bottom seawater Mg concentration (Rouxel et al., 2018).

Table 3. Kama'ehuakanaloa Fluid Magnesium and Chloride Concentrations. Mg and Cl concentrations of Kama'ehuakanaloa fluid samples with corresponding fluid temperature measurements (Milesi et al., 2023). These values are based on samples and data collected during the same cruise (NA100) as the $\delta^{18}O$ and $\delta^{2}H$ values in this study. Synoptic bottom seawater Mg from Pele's Pit were not available, and instead is referenced from measurements made on samples collected in 2007 (Rouxel et al., 2018).

4. Discussion

The stable isotopes of oxygen and hydrogen in water are fractionated as a result of processes occurring throughout the hydrosphere including phase changes and water-rock reactions (Bowers and Taylor, 1985; Chase and Perry, 1972; Craig, 1961). The isotopic structure we observe in the Pacific water-column is an illustration of the cumulative effect of these fractionation processes on the ocean (Fig. 3 & Fig. 5a). Measurements from numerous mid-ocean ridge systems globally have shown that high-temperature vent fluids are typically enriched in ^{18}O relative to ambient seawater and that these fluids are a source of ^{18}O to the oceans (Jean-Baptiste et al., 1997). Less widely reported, measurements of ^{2}H in high-temperature hydrothermal systems also show enrichments relative to seawater in most cases (Campbell et al., 1988; Jean-Baptiste et al., 1997; Shanks et al., 1995). For these reasons, we anticipated that Kama'ehuakanaloa vent fluid samples would exhibit isotopically enriched values relative to ambient seawater at the depth of Pele's Pit. Instead, the opposite was observed - the Caldera Floor vents were isotopically lighter in both $\delta^{18}O$ and $\delta^{2}H$ values than ambient Pacific seawater at the same depth. Notably, however, the hydrothermal system at Kama'ehuakanaloa seamount is quite distinct from the hydrothermal systems that have been investigated more frequently at mid-ocean ridges. First, the Kama'ehuakanaloa hydrothermal vent fluid temperatures observed in this study are low, 40°C or less, and representative of a decades long trend to cooler vent fluids from the maximum of 200°C observed soon after the most recent volcanic eruptions at Kama'ehuakanaloa in 1996 (Wheat et al., 2000). Second, the Mg, Cl, Na, sulfate, and K of Kama'ehuakanaloa vent samples are close to that of seawater (Karl et al. 1988; Rouxel et al. 2018; Milesi et al., 2023); vent fluid chemistries from samples collected at

the time of this study are reported in Milesi et al. (2023) and the Mg and Cl values are included in Table 3 for reference. Third, Kama‘ehuakanaloa, as an intraplate seamount, has a far steeper bathymetric profile across its subsurface hydrothermal flow path than is the case for mid-ocean ridge systems. Mid-ocean ridge systems, therefore, do not necessarily provide suitable analog systems for understanding $\delta^{18}O$ and $\delta^{2}H$ compositions of vent fluids at Kama‘ehuakanaloa.

Among the four groups of fluids, we observed at Kama‘ehuakanaloa, six of the “Caldera seawater” samples (Table 2. NA100-013, NA100-016, NA100-017, NA100-018, NA100-050, NA100-052) stand out for being isotopically heavier in either or both $\delta^{18}O$ and $\delta^{2}H$ values than ambient Pacific seawater at the depth of Pele’s Pit; while the “Crater Floor” vent samples stand out for being isotopically lighter in both $\delta^{18}O$ and $\delta^{2}H$ values than ambient Pacific seawater at the same depth. Taken at face value, the heaviest “Caldera seawater” samples appear consistent with what observations and models predict for high-temperature mid-ocean ridge vent fluid $\delta^{18}O$ and $\delta^{2}H$ values (Bowers and Taylor, 1985). However, when also compared to high-temperature vent fluids, the “Crater Floor” samples exhibit $\delta^{18}O$ and $\delta^{2}H$ values that are lighter than expected. So our results indicate multiple subsurface fluid transport pathways and histories. In one set of samples, the “Crater Floor” vents, we observe isotopic compositions well below what we expect from previous models. In another, the heavy “Caldera seawater” samples, we observe isotopic compositions more consistent with Mid-Ocean Ridge models but located in the water-column at 8 m to 37 m above the caldera floor and not clearly attributable to any currently known seafloor sources. In other sets of samples, the “Crater Rim” and “Chimlet” vents, we observe compositions indicative of subsurface mixing of the “Crater Floor” and “Caldera seawater” fluid types or representative of only partial modification by subsurface processes that proceed further in other systems, or modification by subsurface processes where the initial recharging seawater is isotopically lighter in both $\delta^{18}O$ and $\delta^{2}H$ values than ambient Pacific seawater at the depth of Pele’s Pit. In fact, the isotopic composition of the “Caldera Floor”, “Caldera Rim”, “Chimlet”, and “Caldera seawater” samples stand out more in comparison to that of Pacific Ocean seawater at the same depth (Fig. 4a&b) than they do to the general relationship between seawater $\delta^{18}O$ and $\delta^{2}H$ values in this region (Fig. 5b). Figure 5 shows that the isotopic composition of “Crater Floor”, “Crater Rim”, “Chimlet” and “Caldera seawater” samples generally follow the Pacific seawater $\delta^{18}O$ and $\delta^{2}H$ trend line, except that for all the “Crater Floor”, “Crater Rim”, and “Chimlet” samples, there is a consistent offset toward lower δ2H/higher δ18O values. “Crater Rim” sample NA100-062 falls furthest away from the general trend line. Collectively, these observations suggest that Kama‘ehuakanaloa differs from mid-ocean ridge systems in either or both of the following: (A) processes occurring within the hydrothermal system modify the isotopic composition of entrained seawater, and/or (B) the initial isotopic composition of the entrained seawater. Below, we discuss the water-rock reactions, mantle contributions, and water-microbial mat reactions that may explain our observations (*section* 4.1); and then provide our assessment of the relative importance of these processes at Kama‘ehuakanaloa (*section* 4.2). Section 4.3 will discuss the isotopic sources that constrain our samples.

4.1. Hydrothermal processes that can influence oxygen and hydrogen isotopic ratios in seawater

Water-rock reactions: The isotopic composition of seawater entrained into hydrothermal flow systems are modified by water-rock reactions therein, but the temperatures within the flow system are a key control on the result. Bowers and Taylor, (1985) developed a detailed thermodynamic model of the reactions between seawater and basalt and their influence on the isotopic composition of vent fluids at 21°N East Pacific Rise (EPR). The temperatures that occur along the hydrothermal flow path are important controlling parameters that determine the isotopic results of the process. In the case of $\delta^{18}O$, the model results indicate that temperatures must be sustained >300°C for much of the hydrothermal flow path for water-rock reactions to result in ^{18}O enrichment of the fluid. Moreover, if temperatures in the hydrothermal flow path are <250°C, alteration minerals may instead become enriched in ^{18}O while the fluid becomes depleted. In the case of $\delta^{2}H$, the model results indicate that ^{2}H enrichment of the fluid occurs at all temperatures. However, Bowers and Taylor, (1985) only explicitly modeled reaction paths with temperatures >100°C. At lower reaction temperatures the kinetics of the water-rock reactions become progressively slower and their influence less pronounced. Bowers and Taylor, (1985) also concluded that the water-rock ratio is an important related factor influencing the resulting isotopic composition of the fluid, where lower water-rock ratios, typically associated with higher temperatures, increase water-rock reactions and result in greater enrichments in both isotopic ratios. If subsurface temperatures in the hydrothermal flow path are great enough for phase separation, then the isotopic composition of the hydrothermal fluid may be further fractionated between vapor and liquid phases (e.g., Von Damm et al., 1997). However, there is no indication of phase separation currently occurring at Kama‘ehuakanal□a; vent temperatures are low and vent fluid chloride concentrations are typical of seawater (Table 3; Karl et al. 1988; Rouxel et al. 2018; Milesi et al., 2023). At Kama‘ehuakanaloa, lower temperatures over the course of the hydrothermal flow system could significantly reduce the enrichment of both ^{18}O and ^{2}H relative to that observed at typical mid-ocean ridge systems. Lo’ihi, being a low water:rock system, i.e. ≧1 (Milesi et al., 2023), then water-basalt reactions could have a negligible effect on the isotopic composition of fluids at Kama‘ehuakanaloa. Further, if the temperature of the flow system is <250°C then the $\delta^{18}O$ of the fluid could actually be reduced relative to the entrained seawater, even while the $\delta^{2}H$ is enriched (Bowers and Taylor, 1985). An analogous modeling approach by Böhlke and Shanks, (1994) reached similar conclusions to Bowers and Taylor, (1985) regarding the influence of seawater-basalt reactions on vent fluid isotopic composition.

Mantle Contributions: The isotopic composition of fluid within hydrothermal flow systems can also be modified by the addition of magmatic water with distinct isotopic compositions. Boettcher and O’Neil, (1980) estimated the isotopic composition of deep mantle-derived water to have $\delta^{18}O$ values between +5‰ and +5.9‰ and $\delta^{2}H$ values between -58‰ and -79‰ based on an analysis of kimberlites and xenoliths. The addition of magmatic water to seawater circulating through a hydrothermal flow system would, therefore, tend to increase $\delta^{18}O$ values while simultaneously decreasing $\delta^{2}H$ values from the initial seawater isotopic composition (Shanks et al., 1995). As shown in Fig.5b there is no evidence of any such trend in the Lo’ihi

samples, with the possible exception of “Crater Rim” sample NA100-062. This may seem surprising since recent GEOTRACES investigations have revealed, Kama‘ehuakanaloa to be a significant source of mantle-derived ^{3}He to the Pacific Ocean (Jenkins et al., 2020 and refs therein). This apparent dichotomy may be explained by the observation of Dixon and Clague (2001) that while Kama‘ehuakanaloa basalts exhibit some of the highest known $^{3}He/^{4}He$ anomalies globally, their water content is relatively low. Further, the solubility, in basalt, of water is greater than that of He to the extent that the input of He is likely dominated by degassing deep below the seafloor, while water in seafloor basalt lavas at the summit of Kama‘ehuakanaloa is still undersaturated at that depth (Dixon and Clague, 2001).

Water-Microbial interactions: Kama‘ehuakanaloa is sufficiently different from other hydrothermal systems that other less characterized processes may also influence the isotopic composition of its fluids. In particular, Kama‘ehuakanaloa’s caldera is notable for pronounced microbially mediated iron-oxide deposits associated with the Fe-rich vent fluids surrounding rocky hydrothermal orifices (Breier et al., 2012; Edwards et al., 2011; Emerson and Moyer, 2002; Glazer and Rouxel, 2009; Rouxel et al., 2018). Another possibility, therefore, is that these biotic iron mineral forming mats, or analogous subsurface deposits, may influence the isotopic composition of waters at Kama‘ehuakanaloa. Ferrihydrite is the primary iron mineral in Kama‘ehuakanaloa mats (Toner et al., 2012). While we did not find ^{18}O and ^{2}H isotope fractionation factors specific to ferrihydrite in our review of the literature, we did for laboratory-derived isotope fractionation factors for other iron-oxides. Specifically, evidence from laboratory abiotic synthesis experiments for hematite, akaganeite, and goethite precipitates indicate the ^{18}O isotope fractionation factor for iron minerals is inversely related to temperature, and typically results in a ^{18}O enrichment of the fluid, of 1‰ to 2‰, over a studied temperature range of 35°C to 140°C, and can transition to a decrease in fluid ^{18}O values at temperatures < 35°C (Bao and Koch, 1999). The ^{2}H fractionation factor for goethite has been found to be 0.9 and invariant with temperature indicating ^{2}H enrichment in the fluid phase (Yapp, 2001; Yapp and Pedley, 1985). The fluid temperatures at the “Crater Floor” and “Crater Rim” vents (~11 to 40°C) suggest that iron mineral-fluid isotopic exchange could occur at a range of temperatures for which fluid ^{18}O values could either be reduced or enriched, but that fluid ^{2}H values may only be enriched. There is, however, insufficient information to quantify this potential influence. It has not been observed in a natural setting to our knowledge; and the differences between the chemistry, kinetics, microbiology, and physical environment at Kama‘ehuakanaloa and the laboratory experiments just described are substantial. In addition, the laboratory experiments are conducted in sterile environments to not accommodate for microbial fractionation, further contrasting to Kama‘ehuakanaloa where Fe-oxides are a product of microbial interactions. This is a point that deserves further study and perhaps specifically at Kama‘ehuakanaloa.

429

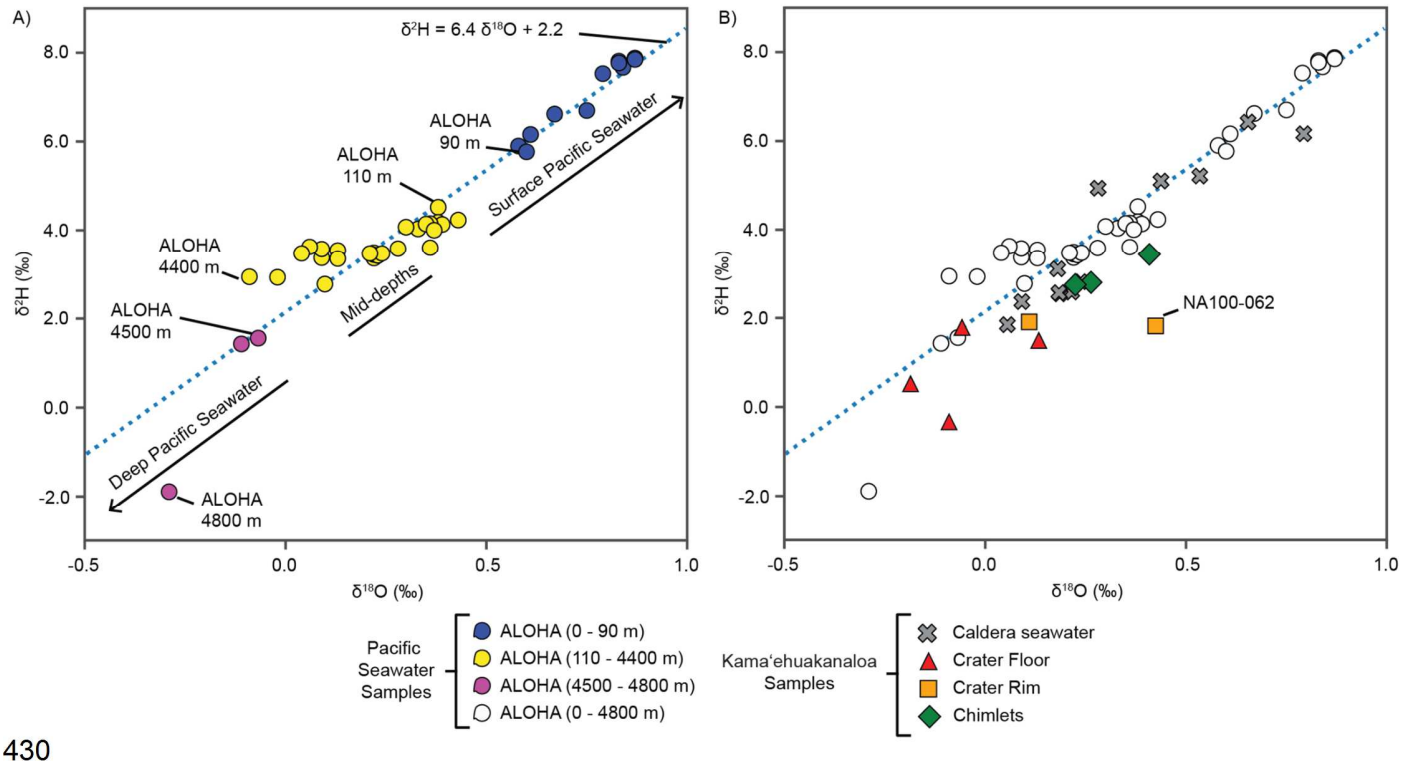

430

431 **Fig. 5. Trends in Pacific Seawater Composition Compared to Kama'ehuakanaloa**
432 **Samples.** A.) The isotopic composition of Pacific seawater at station ALOHA follows a linear
433 trend (dashed blue line) with lighter isotopic $\delta^{18}O$ and $\delta^{2}H$ values as depth increases. B.) The
434 isotopic composition of "Crater Floor", "Crater Rim", "Chimlet" and "Caldera seawater" samples
435 generally follow this same trend, with the caveats that (i) all "Crater Floor", "Crater Rim", and
436 "Chimlet" samples fall on or below the Pacific seawater trend line, and (ii) they typically differ in
437 composition of Pacific seawater from the same depth.

438 [Color image intended for double column width 190 mm, shown at 100% scale]

439

440 *4.2. Processes that influence oxygen and hydrogen isotopic ratios in seawater at*
441 *Kama'ehuakanaloa*

442 The observation that at least six "Caldera seawater" samples from within Pele's Pit are
443 isotopically heavier than ambient seawater from the same depth initially appears consistent with
444 previous observations at high-temperature hydrothermal systems. However, such an
445 interpretation appears to conflict with the measurements we have made from the vent-fluids
446 collected from the vent-sites that we have identified and sampled to date, located at the base of
447 the caldera wall in the SE corner of Pele's Pit and also from vents associated with the north and
448 south rims of the crater (Table 2, Fig. 4). Specifically, the isotopically heavy "Caldera seawater"

samples cannot be explained by simple mixing between these *known* vent-site samples and Pacific seawater from depths of 500-1500 m, all of which are isotopically lighter. What we do note, however, is that these heavy "Caldera seawater" samples were collected from above the seafloor toward the deepest central portion of the Pele's Pit crater, at heights of 8-45m off-bottom and at lateral distances of ≥70m inward, away from the base of the crater wall where the crater-floor vent-sites are located and were sampled. As such, they would not be expected to be entrained into any plume that rises above the more focused venting seen in the vicinity of the Spillway region and could, instead, reflect separate inputs from the central crater floor, whether from additional vents, yet to be located, that lie more directly above the underlying magmatic chamber or akin to the ultra-diffuse venting observed percolating through microbial mat deposits on the deep outer flanks of Kama'ehuakanaloa seamount (Edwards et al., 2011; Rouxel et al., 2018). To produce such an isotopic anomaly at these elevations above the seafloor, at least one of the end-member isotopic values of the fluids, or the net fluid flux, or both, would have to be large relative to the fluxes of the isotopically lighter vent fluid samples. Moreover, the discharge temperatures would also presumably be relatively low. For perspective on the implications, we can establish some constraints on the potential fraction of vent fluid in these samples with a simple mixing model between seawater, using a value of $\delta^{18}O$ = 0.2‰ for Pacific seawater between 1300 m and 1200 m (Table 2), the $\delta^{18}O$ values of these "Caldera seawater" samples, and an assumed source vent fluid. For this, we will start with the assumption that "Caldera seawater" sample NA100-018, with the heaviest $\delta^{18}O$ value of 1.15‰, taken at a depth of 1319 m within 1 m of the caldera floor, is most reflective of the unknown vent fluid $\delta^{18}O$ composition. With that assumption, then "Caldera seawater" sample NA100-016, with a $\delta^{18}O$ value of 0.79‰, taken at a depth of 1275 m and elevation of 45 m above the caldera floor, would include a vent fluid fraction of 62% using equation 1, where $\delta^{18}O_{mix}$ = 0.79‰, $\delta^{18}O_{sw}$ = 0.20‰, and $\delta^{18}O_{vf}$ = 1.15‰. More likely, the vent fluid $\delta^{18}O$ value would be greater than that of NA100-018, already 1 m above the seafloor; if double that of NA100-018, then the vent fluid fraction present in sample NA100-016 would reduce to 28%. Regardless, if these heavy "Caldera seawater" samples are the result of mixing with vent fluid then these would be very high vent fluid fractions at such elevations above the seafloor when compared to the buoyant plumes of mid-ocean ridge "black smokers" and would, instead, be more consistent with large, distributed flows of water exiting the seafloor and heterogeneous mixing. High flows of this nature would be reminiscent of the discharge from the meters wide orifice at the spire of the Von Damm hydrothermal mound on the Mid-Cayman rise, the plume of which undergoes relatively little dilution in the first 8 m (e.g., 77 °C at 1 m plume elevation, 18 °C at 8 m plume elevation: Breier et al. 2014). Alternatively, these heavy isotopic values may reflect the influence of water-mineral reactions such as those just discussed, which may be most detectable in the deepest part of Pele's Pit where limited mixing and the influence of iron-oxide formation may be most pronounced. More data from the water-column and microbial mat interstitial waters within and

around Pele's Pit is needed to better understand what produces the isotopically heavy "Caldera seawater" samples.

The isotopic exchange processes that may occur at Kama'ehuakanaloa tend to enrich one or both ^{18}O and ^{2}H relative to the recharge source. However, the Kama'ehuakanaloa "Crater Floor" samples are isotopically lighter in both $\delta^{18}O$ and $\delta^{2}H$ values than ambient Pacific seawater at the depth of Pele's Pit. We cannot rule out that a combination of the isotopic exchange processes just discussed could produce these fluids, but that would seem to require an unlikely scenario of (i) magmatic volatile contributions large enough to cause a light $\delta^{2}H$ anomaly, coupled with (ii) a thermal history sufficiently low in temperature that water-rock reactions negate the otherwise positive $\delta^{18}O$ magmatic volatile influence. We have insufficient information to constrain whether this could quantitatively result in the observed "Crater Floor" isotopic values. However, those values *can* be readily explained by a Pacific Deepwater recharge source only slightly modified in isotopic composition, if at all. Given the observed Pacific Ocean isotopic structure, only deep Pacific seawater (>4500m) would be sufficiently light in both ^{18}O and ^{2}H to account for the "Crater Floor" vent-fluid isotopic compositions reported here. In this case, isotopic exchange processes may well occur to some extent during hydrothermal circulation, and this would be in keeping with the downward shift of most Kama'ehuakanaloa samples relative to the Pacific Ocean $\delta^{18}O$ vs $\delta^{2}H$ trend shown in Fig. 5b. This could also suggest that the low fluid temperatures observed in the "Crater Floor" vents, which were all 40°C or less, reflect a fluid thermal history where neither subseafloor residence times, nor temperatures were ever sufficient to strongly modify the isotopic composition of the hydrothermal fluid. More specifically, the model of Bowers and Taylor (1985) suggests the fluids discharged from the "Crater Floor" vents may not have exceeded 300°C. However, if the recharge source lies at the greatest depths sampled here (4800 m) with $\delta 18O$ = -0.29‰ and δH = -1.9‰, then the isotopic composition could be modified by hydrothermal processes and still result in the "Crater Floor" vent isotopic compositions.

Milesi et al. (2023) reported a fuller geochemical analysis of the vent fluids sampled during this same cruise and reaction path modeling of the subsurface reactions influencing the "Crater Floor" vent fluids. The findings of Milesi et al. (2023) are also consistent with multiple flow paths. Given the multiple isotopic groupings observed in this study, we recommend that future studies treat each vent grouping as distinct, perform a full chemical intercomparison and analysis of the fluids, and further investigate the extent of diffuse flow venting within the caldera. We also note that our observations represent only an instance in time. Geologically active submarine hotspots may exhibit volcanic eruptive cycles on timescales that are as short as decades (e.g., German et al., 2020; Staudigel et al., 2006; Wheat et al., 2000). It would be very interesting to know the short- and long-term variability of the isotopic composition of the vent fluid and the water within the caldera. Over the eruptive cycles of the volcano, the relative importance of the processes controlling the isotopic composition of the vent fluid are sure to vary and may provide some indication of changes within the system. For now, we will focus on the conclusion that the isotopic composition of Kama'ehuakanaloa "Crater Floor" samples predominantly reflects the $\delta^{18}O$ and $\delta^{2}H$ values of recharging seawater sourced from the deep Pacific.

For the remainder of the discussion, we assume that the “Crater Floor” isotopic values are the result of deep Pacific seawater recharge. In that case, then the fact that these Kama‘ehuakanaloa vent fluids are isotopically light relative to ambient seawater, in contrast to mid-ocean ridge vent fluids that are typically isotopically heavy, is a consequence of a recharge path that is influenced by the much steeper bathymetry of this intraplate volcano relative to mid-ocean ridges. From the caldera floor in Pele’s Pit at a depth of 1320 m, Kama‘ehuakanaloa’s flank descends to abyssal plain depths of 5000 m over a lateral distance of just 20 kilometers. In comparison, starting from the 9° 50’ N EPR axial ridge axis (2,500 m deep), seafloor depths of 5000m are not reached until distances of several hundred kilometers off-axis, at a minimum. It is much further until the EPR ridge flank broadly transitions to depths of 5,000 m. From recharge to discharge, a hydrothermal subsurface flow cell that is on the order of 20 kilometers in lateral offset is entirely consistent with findings from previous studies of subseafloor hydrogeologic processes associated with seafloor venting (*e.g.*, Fisher et al., 2003; Wheat and Fisher, 2008; Tsuji et al, 2012); but in most mid-ocean ridge settings the distance to recharge depths that are significantly deeper and isotopically distinct from discharge depths is likely prohibitive.

4.3. Isotopic source constraints on hydrothermal recharge

Figure 4 shows the linear relationship between $\delta^{18}O$ and $\delta^{2}H$ for the ALOHA station samples. Figure 4 also illustrates how these samples group with the depth of known water masses in this region of the Pacific, specifically: North Pacific Subtropical Water (NPSTW), Subtropical Mode Water (STMW), North Pacific Intermediate Water (NPIW), Antarctic Intermediate Water (AAIW), North Pacific Deep Water (NPDW), and Pacific Bottom Water (PBW). NPSTW extends from the surface to 200 m and STMW from 200 m to 500 m (Cannon, 1966; Masuzawa, 1972; McCartney, 1982). In the intermediate depths, NPIW extends from 500 m to 800 m and then transitions to AAIW which extends to 3000 m (Sverdrup et al., 1942; Talley, 1993; Tsuchiya, 1991). In the deepest depths of the Pacific, Lukas and Santiago-Mandujano, (1996) concluded that North Pacific Deep Water (NPDW) occupies a narrower depth range between 3000 m to 4000 m. The water mass below 4000 m is described as Pacific Bottom Water (PBW) (Lukas and Santiago-Mandujano, 1996). When grouped by the depth boundaries of these water masses there is relatively little isotopic overlap between the ALOHA station samples because they become monotonically lighter with depth with the exception of one $\delta^{18}O$ measurement at a depth of 2600 m (Fig. 6, Table 1). The boxplots in Figures 3C & D representing the ALOHA station samples are also grouped by these depth bands.

As noted, the $\delta^{18}O$ and the $\delta^{2}H$ values of Kama‘ehuakanaloa "Crater Floor" samples are closest in value to the deepest Pacific seawater from >4500 m. We carried out a K-means clustering analysis using the ALOHA dataset and “Crater Floor” samples to show the relationship between the hydrothermal fluid isotopic composition and Pacific water-column isotopic composition. In this analysis, the K-means algorithm grouped the ALOHA station samples into clusters based on the Euclidean distance between individual samples and each cluster centroid in the variable space of $\delta^{18}O$ and the $\delta^{2}H$. Depth was excluded as an explicit variable in the cluster assignments. Three clusters (K=3) were used to group the ALOHA water-column data, because the use of any higher number of clusters resulted in the deepest cluster containing only one sample (Fig. 6). We also calculated the centroid for the “Crater Floor” samples and determined

the Euclidean distances between the “Crater Floor” centroid and the three ALOHA cluster centroids. In Fig. 6,

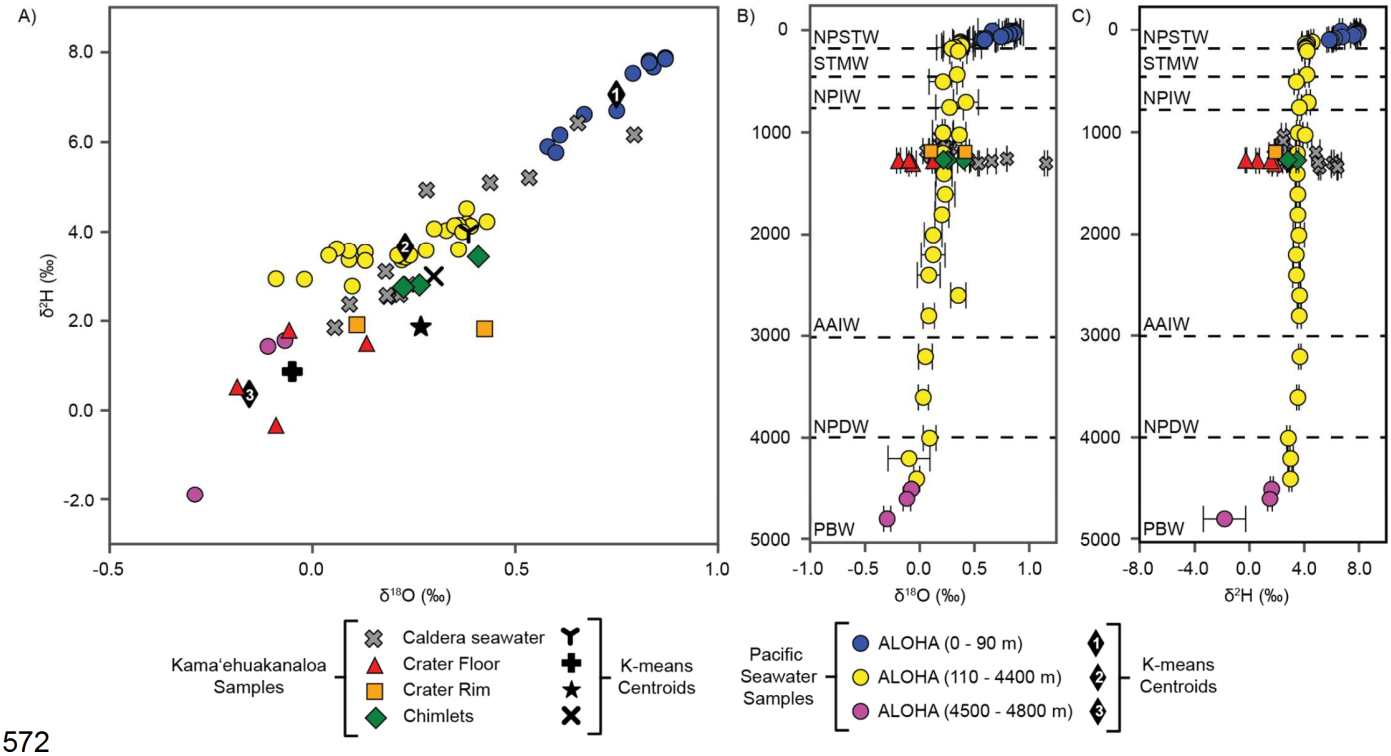

Fig. 6. Isotopic Clusters within Kama‘ehuakanaloa Fluids and Pacific Seawater. A.) Results of K-Means clustering analysis of $\delta^{18}O$ and $\delta^{2}H$ from ALOHA data with a parameterization of 3 clusters. The “Crater Floor”, “Crater Rim”, and “Chimlet” samples are superimposed on the ALOHA data to compare the similarity of ^{18}O and ^{2}H content to ALOHA samples. B.) The $\delta^{18}O$ of Kama‘ehuakanaloa samples are represented at the corresponding depths of Pacific water-column samples. “Crater Floor” samples show a negative deviation from the background Pacific water-column but show similar $\delta^{18}O$ to the deepest Pacific measurements. The “Caldera seawater” samples exhibit more enriched $\delta^{18}O$ than Pacific water-column samples. C.) The $\delta^{2}H$ of Kama‘ehuakanaloa samples are shown at corresponding depths of Pacific water-column $\delta^{2}H$ measurements. Compared to the Pacific water-column samples, “Crater Floor” samples trend to lighter values while “Caldera seawater” samples trend to heavier values. B. and C.) Horizontal dashed lines show regional water mass delineations.

[Color image intended for double column width 190 mm, shown at 100% scale]

the “Crater Floor” samples are shown superimposed on the ALOHA dataset, illustrating that the “Crater Floor” centroid falls closest to the deepest ALOHA cluster centroid with a Euclidean distance of 0.5, as opposed to the next closest ALOHA station cluster centroid with a Euclidean distance of 2.8. This suggests that the “Crater Floor” hydrothermal fluid samples are most similar to the deepest (>4500 m) Pacific water samples from ALOHA Station. Therefore, we

conclude that seawater discharging from the Kama‘ehuakanaloa “Crater Floor” vents originates as Pacific Bottom Water (PBW) from an ocean depth >4500 m that is then discharged ~3500 m shallower at the summit of Kama‘ehuakanaloa seamount. Further, based on our isotopic data, this deep Pacific seawater appears undiluted by mixing with any shallower Pacific Ocean water prior to discharge from the Kama‘ehuakanaloa vent-sites.

The “Crater Rim” and “Chimlet” vents, and some “Caldera seawater” samples, have isotopic values heavier than the “Crater Floor” vents. These samples do not cluster with the isotopic composition of deep Pacific seawater (Fig. 4). This may reflect the influence of isotopic modification processes, including water-rock reactions, on the composition of the same deep Pacific seawater. It may also reflect an overall shallower depth of recharge for these fluids or subsurface mixing of seawater from different depths along the seamount flank. In the case of the heavy “Caldera seawater” samples isotopic modification processes do appear to be necessary to explain the isotopic values, which would otherwise only be similar to Pacific seawater from depths too shallow to mix with these samples.

We expected individual vent fluid isotopic compositions to indicate some combination of subsurface isotopic modification, and entrainment and mixing of seawater through the seamount flank over a greater depth range. And this may be the case for the “Crater Rim”, “Chimlet”, and some of the “Caldera seawater” samples. However, for the “Crater Floor” samples, that does not appear to be the case. These samples appear to illustrate how the seamount provides a natural conduit that siphons Pacific Bottom Water up from the base of the seamount through its hydrothermal flow system and discharges that water at the depth of Pele’s Pit into the much shallower depth range of Pacific intermediate waters. This interpretation appears to be consistent with the bathymetry of the seamount and the nature of the seafloor comprising it. The base of the seamount is in the depth range of 4500 to 5000 m and the geologic interpretation of sidescan sonar by Holcomb et al., (2004) indicates that the base of Kama‘ehuakanaloa in this depth range consists of lava fields and slumps as opposed to intact flanks. Figure 7 illustrates both the regional geological context and the distribution of lava fields, intact flanks, slumps, and areas of debris around Kama‘ehuakanaloa in detail. Any recharge through seafloor deeper than 4500 m would entrain isotopically light seawater. However, away from the immediate base of the seamount the seafloor transitions to sedimented abyssal seafloor at all depths >5000m, covered by fine debris, the archipelagic apron, and ultimately marine sediments. The potential flow-path for recharge through this distal zone is depicted in Figure 7 using yellow arrows. Flow through this path is anticipated to be low, due to low hydraulic conductivity controlled by the sediment cover unless cross-cutting faulting is present (e.g., Tsuji et al. 2012). In contrast, the lava fields and slumps that comprise the base of Kama‘ehuakanaloa’s flanks are expected to contain a high concentration of fractures and conduits resulting in areas of relatively high hydraulic conductivity where seawater can more readily recharge the hydrothermal flow network. This potential flow-path is depicted in Figure 7 using red arrows. Such recharge could represent the start of a family of flow paths that pass through the Kama‘ehuakanaloa subsurface hydrothermal flow network and thereby produce the diverse range of fluids observed at the summit. One of these flow paths appears to rise through the volcano with relatively little isotopic alteration to be discharged at the “Crater Floor” vents.

Thus, our studies present a novel mechanism for vertical ocean mixing in which lithospheric thermal energy has the potential to transport seawater upwards of 3200 m in the ocean. This could represent a hydrothermally driven short-circuit in ocean mixing that could not occur at mid-ocean ridges, but may be common to all intra-plate seamounts, not just those associated with hot-spot systems of the kind investigated here. The speciation of Fe in the Kama‘ehuakanaloa plume, which allows it to be dispersed over long distances, is an active area of research. This study helps inform the processes that must contribute to setting the export flux from Lo’ihi to the surrounding ocean. As noted, Kama‘ehuakanaloa’s flank descends to 5000 m in 20 km, whereas the shallow slopes of mid-ocean ridges, away from transform faults, require 100s to 1000s of km to reach similar depths. Hydrothermal flow through inactive seamounts, driven by lithospheric heat, has been proposed previously based on heat flow and sediment porewater observations (Wheat et al., 2019). Our data illustrates a lithospheric heat-driven hydrothermal flow system in an active volcano, based on a different and independent set of parameters: the isotopic composition of the vent fluid and seawater.

Kama‘ehuakanaloa is an active hot-spot related volcano with sufficient heat and hydrothermal discharge to distribute helium-3 and iron across long spatial scales within the Pacific (Jenkins et al., 2020; Lupton, 1996). In fact, the modeling results of Jenkins et al. (2020) predict the dispersal and circulation of Kama‘ehuakanaloa hydrothermal iron through the upper layers of the north Pacific, even into the shallow northwest Pacific. While the number of similar active hot-spot volcanoes is limited, the thermal power of these submarine volcanoes and the shallow depths at which their hydrothermal systems discharge give them the potential to influence marine geochemical budgets in a particularly effective manner. Our results provide particular insights into where seawater is entrained into the Kama‘ehuakanaloa hydrothermal circulation system but may also be relevant to numerous other topographic basement features across the ocean floor including island arc and intra-plate seamounts, not just ocean island hotspots.

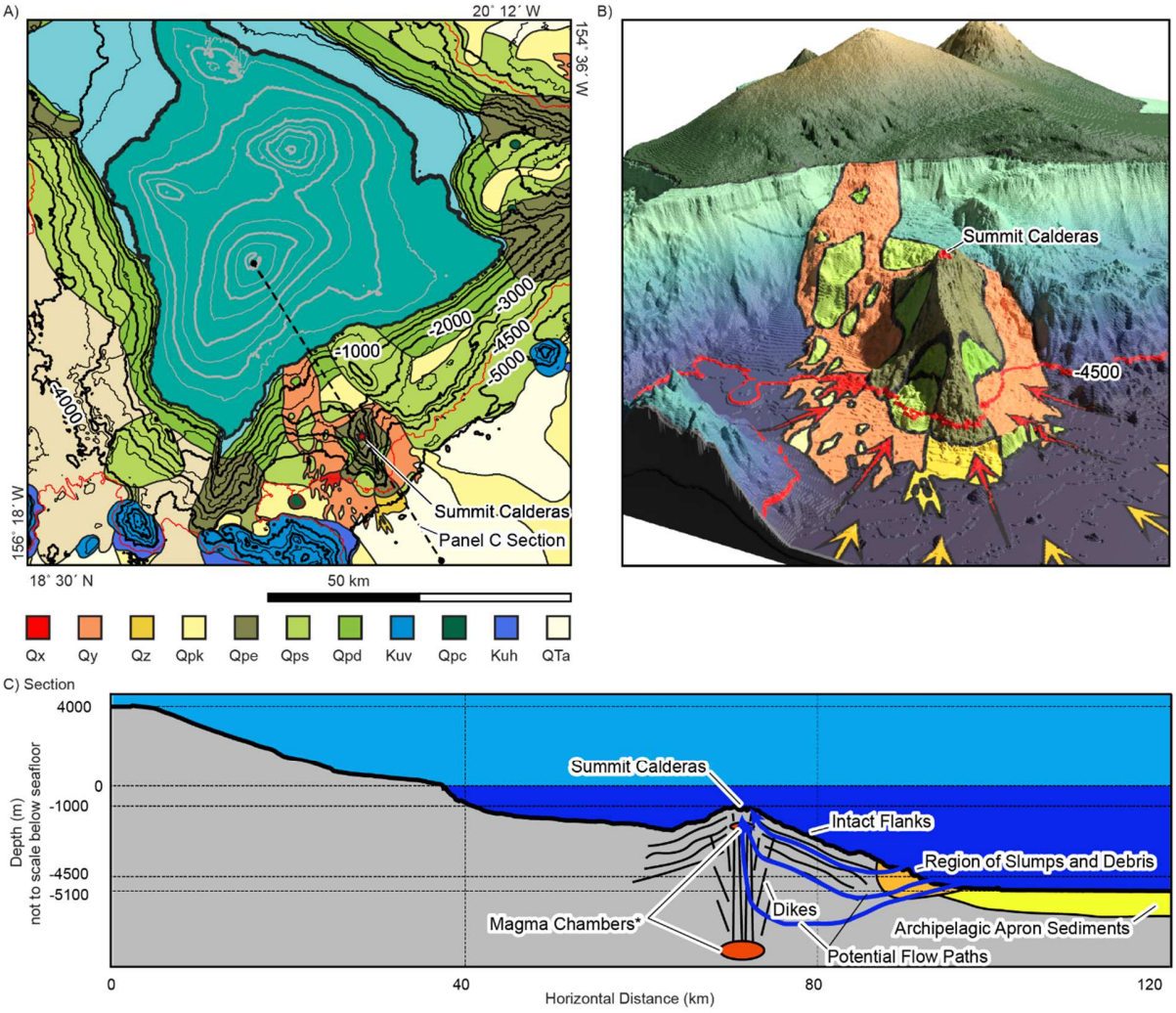

Fig. 7. Geological Context of Kama‘ehuakanaloa Seamount with Potential Recharge Zones. A.) Regional geological interpretation from Holcomb et al., (2004): Qx, Qy, and Qz are lava fields of strong, intermediate, and weak sonar backscatter; QpK are fine debris avalanche areas; Qpe are intact flanks; Qps are slumps; Qpd are debris flanks; Kuv and Qpc are large and small volcanoes; Kuh is volcanic terrain; and QTa is archipelagic apron. Bathymetry is from Ryan et al., (2009); contours are at 500 m intervals. B.) Our results suggest recharge to the Kama‘ehuakanaloa hydrothermal system is primarily occurring below 4500 m (indicated by the red line of bathymetry), which intersects the base of Kama‘ehuakanaloa where it is surrounded by lava fields (Qx, Qy, and Qz) and slumps (Qps). This potentially creates a region of higher hydraulic conductivity where recharge is more probable, and that possibility is depicted here with red arrows. Recharge through deeper seafloor is also possible and is depicted by yellow arrows. C.) This section through Kama‘ehuakanaloa (corresponding to section line shown in panel A) illustrates how recharge to the hydrothermal flow system may be preferentially guided through the zone of slumps and debris at the base of the seamount and follow different flow paths through the volcano. *Note depth, size, and number of magma chambers and locations of

675 dikes and flank layers are for conceptual illustration only actual internal details are not known to
676 this degree and may differ.

677 [Color image intended for double column width 190 mm, shown at 100% scale]

678 **5.0 Conclusions**

679 Our observations suggest that hydrothermal fluids at Kama‘ehuakanaloa follow multiple different
680 subsurface transport pathways that span a range of thermal trajectories. In particular, the (i)
681 isotopically heavy “Caldera seawater” samples and the (ii) isotopically light "Crater Floor"
682 samples stand out with respect to ambient Pacific seawater at the depth of Pele's Pit. The
683 isotopically heavy “Caldera seawater” samples are predominantly from the caldera's deepest
684 depths, but no seafloor endmember with similar isotopic composition was found. Therefore, we
685 infer there may be additional sources of hydrothermal discharge within the caldera, potentially
686 diffuse, that represent the primary hydrothermal component within those samples. In contrast,
687 isotopic exchange processes do not appear sufficient to explain the light $\delta^{18}O$ and $\delta^{2}H$ isotopic
688 values of the "Crater Floor" fluids. Instead, we conclude that the isotopic composition of the
689 "Crater Floor" fluids primarily reflects the isotopic composition of the recharge source, which
690 appears to be Pacific Bottom Water from depths below 4500 m. Flow of this kind would
691 represent a previously unrecognized, hydrothermally driven, mechanism driving vertical mixing
692 in the deep ocean that may be repeated wherever similarly pronounced basement topographic
693 features arise.

694

695 **Acknowledgments**

696 This work was supported by NASA Planetary Science and Technology Through Analog
697 Research (PSTAR) Program (NNH16ZDA001N-PSTAR) grant (16-PSTAR16_2-0011) to DSSL
698 and NOAA-OER grant #NA17OAR0110336 with additional support to JAB from NSF grants
699 OCE-1636510, OCE-1851208, and OCE-1924508 and to CRG from NASA Astrobiology grant
700 #80NSSC19K1427. The NOAA Educational Partnership Program with Minority-Serving
701 Institutions Cooperative Agreement Award #NA16SEC4810009 also provided support to JAB
702 and BAA; the contents of this article are solely the responsibility of the authors and do not
703 necessarily represent the official views of the U.S. Department of Commerce, National Oceanic
704 and Atmospheric Administration. This research used samples provided by the Ocean
705 Exploration Trust’s Nautilus Exploration Program, Cruise NA100. We would like to thank the
706 cruise expedition Leader N. Raineault, the ROV Hercules/Argus team, and the crew of the E/V
707 Nautilus for their assistance while at sea. This publication is based upon preliminary Hawaii
708 Ocean Time-series observations supported by NSF grant OCE-1756517. We would like to thank
709 the cruise leader C. Funkey and crew of the R/V Kilo Moana for their assistance while at sea.
710 We would also like to thank an anonymous reviewer, and the Editor for their constructive
711 suggestions. This is SUBSEA publication SUBSEA-2020-003.

712

Author Contributions

EC: Methodology, Formal Analysis, Investigation, Data Curation, Writing - Original Draft, Writing - Review & Editing, Visualization; BA: Investigation CG: Field Program implementation, Investigation, Writing - Review & Editing, Funding acquisition; DL: Investigation, Writing - Review & Editing, Project Administration, Funding acquisition; JB: Conceptualization, Methodology, Writing - Original Draft, Writing - Review & Editing, Visualization, Supervision, Project administration, Funding acquisition

Declaration of Competing Interests

The authors declare they have no competing interests.

References

Anantharaman, K., Breier, J.A., Dick, G.J., 2016. Metagenomic resolution of microbial functions in deep-sea hydrothermal plumes across the Eastern Lau Spreading Center. ISME J. 10, 225–239. https://doi.org/10.1038/ismej.2015.81

Bao, H., Koch, P.L., 1999. Oxygen isotope fractionation in ferric oxide-water systems: low temperature synthesis. Geochim. Cosmochim. Acta 63, 599–613. https://doi.org/10.1016/S0016-7037(99)00005-8

Boettcher, A.L., O'Neil, J.R., 1980. Stable isotope, chemical, and petrographic studies of high-pressure amphiboles and micas: evidence for metasomatism in the mantle source regions of alkali basalts and kimberlites. Am. J. Sci. 280, 594–621.

Böhlke, J.K., Shanks, W.C., III, 1994. Stable isotope study of hydrothermal vents at Escanaba Trough: Observed and calculated effects of sediment-seawater interaction. In: J.L. Morton, R.A. Zierenberg, C.A. Reiss (Eds.), Geologic, Hydrothermal, and Biologic Studies at Escanaba Trough, Gorda Ridge, Offshore Northern California, U.S. Geological Survey Bulletin 2022, pp. 223-240.

Bowers, T.S., Taylor, H.P., 1985. An integrated chemical and stable-isotope model of the origin of Midocean Ridge Hot Spring Systems. Journal of Geophysical Research. https://doi.org/10.1029/jb090ib14p12583

Breier, J.A., Sheik, C.S., Gomez-Ibanez, D., Sayre-McCord, R.T., Sanger, R., Rauch, C., Coleman, M., Bennett, S.A., Cron, B.R., Li, M., German, C.R., Toner, B.M., Dick, G.J., 2014. A large volume particulate and water multi-sampler with in situ preservation for microbial and biogeochemical studies. Deep Sea Res. Part I 94, 195–206. https://doi.org/10.1016/j.dsr.2014.08.008

Breier, J.A., Toner, B.M., Fakra, S.C., Marcus, M.A., White, S.N., Thurnherr, A.M., German, C.R., 2012. Sulfur, sulfides, oxides and organic matter aggregated in submarine hydrothermal plumes at 9°50′N East Pacific Rise. Geochimica et Cosmochimica Acta. https://doi.org/10.1016/j.gca.2012.04.003

Campbell, A.C., Palmer, M.R., Klinkhammer, G.P., Bowers, T.S., Edmond, J.M., Lawrence, J.R., Casey, J.F., Thompson, G., Humphris, S., Rona, P., Others, 1988. Chemistry of hot springs on the Mid-Atlantic Ridge. Nature 335, 514–519.

Canfield, D.E., Poulton, S.W., Knoll, A.H., Narbonne, G.M., Ross, G., Goldberg, T., Strauss, H., 2008. Ferruginous conditions dominated later neoproterozoic deep-water chemistry. Science. https://doi.org/10.1126/science.1154499

Cannon, G.A., 1966, December. Tropical waters in the western Pacific Ocean, August–September 1957. In: Deep Sea Research and Oceanographic Abstracts, 13(6): 1139–1148, doi: https://doi.org/10.1016/0011-7471(66)90705-4

Chase, C.G., Perry, E.C., Jr, 1972. The oceans: growth and oxygen isotope evolution. Science 177, 992–994. https://doi.org/10.1126/science.177.4053.992

Craig, H., 1961. Isotopic variations in meteoric waters. Science 133, 1702–1703. https://doi.org/10.1126/science.133.3465.1702

Davis, A.S., Clague, D.A., 1998. Changes in the hydrothermal system at Loihi Seamount after the formation of Pele's pit in 1996. Geology 26, 399–402. https://doi.org/2.3.CO;2">10.1130/0091-7613(1998)026<0399:CITHSA>2.3.CO;2

767 Dixon, J.E., Clague, D.A., 2001. Volatiles in basaltic glasses from Loihi Seamount, Hawaii:
768 evidence for a relatively dry plume component. J. Petrol. 42, 627–654.
769 https://doi.org/10.1093/petrology/42.3.627
770 Duennenbier, F.K., Becker, N.C., Caplan-Auerbach, J., Clague, D.A., Cowen, J., Cremer, M.,
771 Garcia, M., Goff, F., Malahoff, A., McMurtry, G.M. and Midson, B.P., 1997. Researchers
772 rapidly respond to submarine activity at Loihi volcano, Hawaii. Eos, 78(22), p.229.
773 Edwards, K.J., Bach, W., McCollom, T.M., 2005. Geomicrobiology in oceanography: microbe–
774 mineral interactions at and below the seafloor. Trends Microbiol. 13, 449–456.
775 https://doi.org/10.1016/j.tim.2005.07.005
776 Edwards, K.J., Glazer, B.T., Rouxel, O.J., Bach, W., Emerson, D., Davis, R.E., Toner, B.M.,
777 Chan, C.S., Tebo, B.M., Staudigel, H., Moyer, C.L., 2011. Ultra-diffuse hydrothermal
778 venting supports Fe-oxidizing bacteria and massive umber deposition at 5000 m off Hawaii.
779 ISME J. 5, 1748–1758. https://doi.org/10.1038/ismej.2011.48
780 Elderfield, H., Schultz, A., 1996. Mid-ocean ridge hydrothermal fluxes and the chemical
781 composition of the ocean. Annual Review of Earth and Planetary Sciences.
782 https://doi.org/10.1146/annurev.earth.24.1.191
783 Emerson, D., Moyer, C.L., 2002. Neutrophilic Fe-oxidizing bacteria are abundant at the Loihi
784 Seamount hydrothermal vents and play a major role in Fe oxide deposition. Appl. Environ.
785 Microbiol. 68, 3085–3093. https://doi.org/10.1128/aem.68.6.3085-3093.2002
786 Emery, W.J., 2001. Water types and water masses. In: .H. Steele, K.K. Turekian, S.A. Thorpe
787 (Eds.), Encyclopedia of Ocean Sciences, Academic Press (2001), pp. 3179-3187
788 Fisher, A.T., Davis, E.E., Hutnak, M., Spiess, V., Zühlsdorff, L., Cherkaoui, A., Christiansen, L.,
789 Edwards, K., Macdonald, R., Villinger, H., Mottl, M.J., Wheat, C.G., Becker, K., 2003.
790 Hydrothermal recharge and discharge across 50 km guided by seamounts on a young
791 ridge flank. Nature 421, 618–621. https://doi.org/10.1038/nature01352
792 Garcia, M.O., Rubin, K.H., Norman, M.D., Michael Rhodes, J., Graham, D.W., Muenow, D.W.,
793 Spencer, K., 1998. Petrology and geochronology of basalt breccia from the 1996
794 earthquake swarm of Loihi seamount, Hawaii: magmatic history of its 1996 eruption.
795 Bulletin of Volcanology. https://doi.org/10.1007/s004450050211
796 German, C.R., Resing, J.A., Xu, G., Yeo, I.A., Walker, S.L., Devey, C.W., Moffett, J.W., Cutter,
797 G.A., Hyvernaud, O., Reymond, D., 2020. Hydrothermal activity and seismicity at Teahitia
798 Seamount: reactivation of the Society Islands hotspot? Frontiers in Marine Science 7, 73.
799 https://doi.org/10.3389/fmars.2020.00073
800 German, C.R., Seyfried, W.E., 2014. Hydrothermal Processes. In: H. Elderfield (Ed.), Treatise
801 on Geochemistry: The Oceans and Marine Geochemistry, Elsevier/Pergamon, Oxford,
802 https://doi.org/10.1016/b978-0-08-095975-7.00607-0
803 Glazer, B.T., Rouxel, O.J., 2009. Redox speciation and distribution within diverse iron-
804 dominated microbial habitats at Loihi Seamount. Geomicrobiol. J. 26, 606–622.
805 https://doi.org/10.1080/01490450903263392
806 Robinson, J.E., Hamer, M.R., Stevenson, A.J., Lucky, H., Degnan, C.H., Wong, F.L., Holcomb,
807 R.T., 2004. Digital data for maps of Hawaiian Islands exclusive economic zone interpreted
808 from GLORIA sidescan-sonar imagery. U.S. Geological Survey Scientific Investigations
809 Map 2824

Jaffrés, J.B.D., Shields, G.A., Wallmann, K., 2007. The oxygen isotope evolution of seawater: A critical review of a long-standing controversy and an improved geological water cycle model for the past 3.4 billion years. Earth-Sci. Rev. 83, 83–122. https://doi.org/10.1016/j.earscirev.2007.04.002

Jean-Baptiste, P., Dapoigny, A., Stievenard, M., Charlou, J.L., Fouquet, Y., Donval, J.P., Auzende, J.M., 1997. Helium and oxygen isotope analyses of hydrothermal fluids from the East Pacific Rise between 17°S and 19°S. Geo-Marine Letters. https://doi.org/10.1007/s003670050029

Jenkins, W.J., Hatta, M., Fitzsimmons, J.N., Schlitzer, R., Lanning, N.T., Shiller, A., Buckley, N.R., German, C.R., Lott, D.E., Weiss, G., Whitmore, L., Casciotti, K., Lam, P.J., Cutter, G.A., Cahill, K.L., 2020. An intermediate-depth source of hydrothermal 3He and dissolved iron in the North Pacific. Earth Planet. Sci. Lett. 539, 116223. https://doi.org/10.1016/j.epsl.2020.116223

Johnson, G.C., Toole, J.M., 1993. Flow of deep and bottom waters in the Pacific at 10 N. Deep Sea Res. Part I 40, 371–394.

Johnson, H.P., Tivey, M.A., Bjorklund, T.A., Salmi, M.S., 2010. Hydrothermal circulation within the Endeavour segment, Juan de Fuca Ridge. Geochem. Geophys. Geosyst. 11.

Karl, D.M., Brittain, A.M., Tilbrook, B.D., 1989. Hydrothermal and microbial processes at Loihi Seamount, a mid-plate hot-spot volcano. Deep Sea Res. A 36, 1655–1673. https://doi.org/10.1016/0198-0149(89)90065-4

Karl, D.M., McMurtry, G.M., Malahoff, A. and Garcia, M.O., 1988. Loihi Seamount, Hawaii: a mid-plate volcano with a distinctive hydrothermal system. Nature, 335(6190), pp.532-535. https://doi.org/10.1038/335532a0

Kuroda, Y., Suzuoki, T., Matsuo, S., 1977. Hydrogen isotope composition of deep-seated water. Contrib. Mineral. Petrol. 60, 311–315.

Lin, Y., Clayton, R.N., Gröning, M., 2010. Calibration of δ17O and δ18O of international measurement standards--VSMOW, VSMOW2, SLAP, and SLAP2. Rapid Commun. Mass Spectrom. 24, 773–776.

Lukas, R., Santiago-Mandujano, F., 1996. Interannual variability of Pacific deep- and bottom-waters observed in the Hawaii Ocean Time-series. Deep Sea Res. Part 2 Top. Stud. Oceanogr. 43, 243–255. https://doi.org/10.1016/0967-0645(95)00103-4

Lupton, J.E., 1996. A far-field hydrothermal plume from Loihi Seamount. Science 272, 976–979. https://doi.org/10.1126/science.272.5264.976

Masuzawa, J., 1972. Water characteristics of the North Pacific central region. Kuroshio-Its Physical Aspects, pp.95-127.

McCartney, M.S., 1982. The subtropical recirculation of mode waters. J. Mar. Res, 40(436), pp.427-464.

Milesi, V., Shock, E., Seewald, J., Trembath-Reichert, E. , Sylva, S.P., Huber, J.A., Lim, D.S.S, German, C.R. 2023 Multiple parameters enable deconvolution of water-rock reaction paths in low-temperature vent fluids of the Kama‘ehuakanaloa (Lō‘ihi) seamount. Geochim. Cosmochim. Acta, https://doi.org/10.1016/j.gca.2023.03.013

Neal, C.A., Brantley, S.R., Antolik, L., Babb, J.L., Burgess, M., Calles, K., Cappos, M., Chang, J.C., Conway, S., Desmither, L., Dotray, P., Elias, T., Fukunaga, P., Fuke, S., Johanson, I.A., Kamibayashi, K., Kauahikaua, J., Lee, R.L., Pekalib, S., Miklius, A., Million, W., Moniz,

C.J., Nadeau, P.A., Okubo, P., Parcheta, C., Patrick, M.R., Shiro, B., Swanson, D.A., Tollett, W., Trusdell, F., Younger, E.F., Zoeller, M.H., Montgomery-Brown, E.K., Anderson, K.R., Poland, M.P., Ball, J.L., Bard, J., Coombs, M., Dietterich, H.R., Kern, C., Thelen, W.A., Cervelli, P.F., Orr, T., Houghton, B.F., Gansecki, C., Hazlett, R., Lundgren, P., Diefenbach, A.K., Lerner, A.H., Waite, G., Kelly, P., Clor, L., Werner, C., Mulliken, K., Fisher, G., Damby, D., 2019. The 2018 rift eruption and summit collapse of Kīlauea Volcano. Science 363, 367–374. https://doi.org/10.1126/science.aav7046

Paulmier, A., Ruiz-Pino, D., 2009. Oxygen minimum zones (OMZs) in the modern ocean. Progress in Oceanography, 80(3-4), pp.113-128. https://doi.org/10.1016/j.pocean.2008.08.001

Pedregosa, F., Varoquaux, G., Gramfort, A., Michel, V., Thirion, B., Grisel, O., Blondel, M., Prettenhofer, P., Weiss, R., Dubourg, V., Others, 2011. Scikit-learn: Machine learning in Python. The Journal of Machine Learning Research 12, 2825–2830.

Rison, W., Craig, H., 1983. Helium isotopes and mantle volatiles in Loihi Seamount and Hawaiian Island basalts and xenoliths. Earth Planet. Sci. Lett. 66, 407–426. https://doi.org/10.1016/0012-821X(83)90155-3

Rouxel, O., Toner, B., Germain, Y., Glazer, B., 2018. Geochemical and iron isotopic insights into hydrothermal iron oxyhydroxide deposit formation at Loihi Seamount. Geochim. Cosmochim. Acta 220, 449–482. https://doi.org/10.1016/j.gca.2017.09.050

Ryan, W.B.F., Carbotte, S.M., Coplan, J.O., O'Hara, S., Melkonian, A., Arko, R., Weissel, R.A., Ferrini, V., Goodwillie, A., Nitsche, F., Others, 2009. Global multi-resolution topography synthesis. Geochem. Geophys. Geosyst. 10.

Rye, R.O., 1993. The evolution of magmatic fluids in the epithermal environment; the stable isotope perspective. Econ. Geol. 88, 733–752.

Sedwick, P.N., McMurtry, G.M. and Macdougall, J.D., 1992. Chemistry of hydrothermal solutions from Pele's vents, Loihi Seamount, Hawaii. Geochimica et Cosmochimica Acta, 56(10), pp.3643-3667. https://doi.org/10.1016/0016-7037(92)90159-G

Shanks, W.C., Boehlke, J.K., Seal, R.R., Humphris, S.E., 1995. Stable isotopes in mid-ocean ridge hydrothermal systems: Interactions between fluids, minerals, and organisms. Geophysical Monograph-American Geophysical Union 91, 194–194.

Staudigel, H., Hart, S.R., Pile, A., Bailey, B.E., Baker, E.T., Brooke, S., Connelly, D.P., Haucke, L., German, C.R., Hudson, I., Jones, D., Koppers, A.A.P., Konter, J., Lee, R., Pietsch, T.W., Tebo, B.M., Templeton, A.S., Zierenberg, R., Young, C.M., 2006. Vailulu'u Seamount, Samoa: Life and death on an active submarine volcano. Proceedings of the National Academy of Sciences. https://doi.org/10.1073/pnas.0600830103

Sverdrup, H.U., Johnson, M.W. and Fleming, R.H., 1942. The Oceans: Their physics, chemistry, and general biology (Vol. 1087). New York: Prentice-Hall.

Tagliabue, A., Bowie, A.R., Boyd, P.W., Buck, K.N., Johnson, K.S., Saito, M.A., 2017. The integral role of iron in ocean biogeochemistry. Nature 543, 51–59. https://doi.org/10.1038/nature21058

Talley, L.D., 1993. Distribution and formation of North Pacific intermediate water. Journal of Physical Oceanography, 23, pp.517-517.

Toner, B.M., Berquó, T.S., Michel, F.M., Sorensen, J.V., Templeton, A.S., Edwards, K.J., 2012. Mineralogy of iron microbial mats from Loihi seamount. Front. Microbiol. 3, 118. https://doi.org/10.3389/fmicb.2012.00118

Tsuchiya, M., 1991. Flow path of the Antarctic Intermediate Water in the western equatorial South Pacific Ocean. Deep Sea Research Part A. Oceanographic Research Papers, 38, pp.S273-S279.

Walker, S.A., Azetsu-Scott, K., Normandeau, C., Kelley, D.E., Friedrich, R., Newton, R., Schlosser, P., McKay, J.L., Abdi, W., Kerrigan, E., Craig, S.E., Wallace, D.W.R., 2016. Oxygen isotope measurements of seawater (H218O/ H216O): A comparison of cavity ring-down spectroscopy (CRDS) and isotope ratio mass spectrometry (IRMS). Limnology and Oceanography: Methods. https://doi.org/10.1002/lom3.10067

Wheat, C.G., Fisher, A.T., 2008. Massive, low-temperature hydrothermal flow from a basaltic outcrop on 23 Ma seafloor of the Cocos Plate: Chemical constraints and implications. Geochem. Geophys. Geosyst. 9.

Wheat, C.G., Hartwell, A.M., McManus, J., 2019. Geology and fluid discharge at Dorado Outcrop, a low temperature ridge flank hydrothermal system. Geochem. Explor. Environ. Analy.

Wheat, C.G., Jannasch, H.W., Plant, J.N., Moyer, C.L., Sansone, F.J., McMurtry, G.M., 2000. Continuous sampling of hydrothermal fluids from Loihi Seamount after the 1996 event. J. Geophys. Res., Geophys. Monogr. Ser. 105, 19353–19367. https://doi.org/10.1029/2000JB900088

Yapp, C., 2001. Rusty relics of Earth history: Iron (III) oxides, isotopes, and surficial environments. Annu. Rev. Earth Planet. Sci. 29, 165–199.

Yapp, C.J., Pedley, M.D., 1985. Stable hydrogen isotopes in iron oxides—II. DH variations among natural goethites. Geochim. Cosmochim. Acta 49, 487–495. https://doi.org/10.1016/0016-7037(85)90040-7